INTERNATIONAL JOURNAL OF GEOENGINEERING CASE HISTORIES

Pressure on Walls Retaining Swelling Soils: Numerical Simulations, Case Histories and Design Suggestions

Jean-Louis Briaud – *Professor, Zachry Dpt. of Civil and Environmental Engineering, Texas A&M University, College Station (Texas, USA)*
briaud@tamu.edu

Erick Cruz – *PhD student, Zachry Dpt. of Civil and Environmental Engineering, Texas A&M University, College Station (Texas, USA)*
ecvcruz@gmail.com

Yichi Du – *PhD student, Zachry Dpt. of Civil and Environmental Engineering, Texas A&M University, College Station (Texas, USA)*
ycdu@tamu.edu

Marcelo Sanchez – *Professor, Zachry Dpt. of Civil and Environmental Engineering, Texas A&M University, College Station (Texas, USA)*
msanchez@civil.tamu.edu

ABSTRACT: *The earth pressure on retaining walls is often considered to be the "active pressure" or the "at rest pressure" and may involve the passive pressure. However, in the case of swelling soils and when the top of the wall is inundated for a long period of time, the pressure can be much higher than the active pressure. In this article, the pressure on retaining walls generated by inundated swelling soils is investigated based on well-documented case histories and numerical simulations using unsaturated soil mechanics principles. Because the swell pressure plays a critical role in this case, the swell pressure prediction methods are briefly evaluated. The results of the case histories analysis and associated numerical simulations include the maximum potential pressure diagram, the influence of the wall movement, and the time-dependent pressure diagram. The inundation time is a major influencing factor, and the concept of the 100-year inundation period is developed as a design inundation time. In the unusual case where the inundation period is sustained for a long period of time, the pressure diagram for swelling soils shows a much higher pressure toward the top of the wall compared to non-swelling soils. In this extreme case, a shallow anchor is suggested to resist the pressure on walls retaining swelling soils; a vertical compressible layer to reduce the pressure between the wall and the soil when it swells is another possible solution.*

KEYWORDS: *retaining wall, swelling soil, measurements, pressure, movement, numerical simulations, design*

Submitted: 13 November 2024; Published: 07 July 2026
Reference: Briaud, J.-L., Cruz, E., Du, Y., & Sanchez, M. (2026). Pressure On Walls Retaining Swelling Soils: Numerical Simulations, Case Histories and Design Suggestions. *International Journal of Geoengineering Case Histories, 8*(4), 01–30.
https://doi.org/10.4417/IJGCH-08-04-01

INTRODUCTION

Retaining walls can be classified into two main categories: bottom-up walls such as gravity walls or MSE walls, and top-down walls such as tieback walls or slurry walls. In the case of bottom-up walls, the wall is built from the bottom up by erecting the wall first as a free-standing structure and compacting the backfill in lifts behind the wall. In the case of top down retaining walls, the wall is typically constructed in the ground and, when ready, the soil in front of the wall is excavated with or without the placement of anchors as the excavation depth increases. Clean coarse-grained soils are the backfill of choice for bottom-up retaining walls. However, at times, the retained soil behind a top down retaining wall is a swelling soil. The

DOI: 10.4417/IJGCH-08-04-01

swelling pressure will impact the pressure on the wall should the soil become inundated and swell during the design life of the wall. In this case, this pressure needs to be evaluated and considered. Previous contributions related to this topic include the work of Abdollah and Vahedifard (2021), Fourie (1989), Habib and Karube (1993), Liu et al. (2021), Liu and Vanapalli (2017, 2019), Gu (2005), Mohamed et al. (2013), Zhang et al. (2020), Clayton et al. (1991), Brown (2013), and Katti et al. (1983). This published work represents a mix of theoretical studies, small laboratory tests, centrifuge tests, and a few full-scale instrumented wall projects. These publications were studied in preparation for this research, but preference was given to full-scale measurements.

This article aims to answer the question: what pressure can such walls be subjected to? At first glance, one might think about the swell pressure of the soil. On the other hand, one might think that the movement of the wall would reduce such a pressure. Furthermore, the length of time of inundation behind the wall and the associated change in water content of the soil should affect that pressure. Those factors and more are addressed through a combination of analysis of published case histories and numerical simulations by the finite difference/P-y curve method using RSPILE (2024) on one hand and by the finite element method using CODE_BRIGHT (2023) on the other hand. Because the swell pressure plays an important role in the process, equations to predict the swell pressure are evaluated as well.

GUIDELINES

The number of published guidelines to estimate the pressure on walls retaining swelling soils is very limited. The ones described next are the Canadian Foundation Engineering Manual (2006) recommendations, and the NAVFAC (1986) recommendations. Note that, consistent with classical earth pressure theories and no surcharge at the top of the wall, the total active, passive, and at rest earth pressures at a depth z below the top of the wall are given by (Briaud, 2013a):

$$\sigma_{ah} = K_a \sigma'_{ov} - 2c'\sqrt{K_a} + \alpha u_w \quad (1)$$

$$\sigma_{ph} = K_p \sigma'_{ov} + 2c'\sqrt{K_p} + \alpha u_w \quad (2)$$

$$\sigma_{oh} = K_o \sigma'_{ov} + \alpha u_w \quad (3)$$

where σ_{ah} is the total active earth pressure at depth z, K_a is the coefficient of active earth pressure, σ'_{ov} is the vertical effective stress at depth z, c' the effective stress cohesion, α the water area ratio (1 for saturated soils), u_w is the water stress at depth z, σ_{ph} is the total passive earth pressure at depth z, K_p is the coefficient of passive earth pressure, σ_{oh} is the total at rest horizontal stress at depth z, and K_o is the coefficient of earth pressure at rest. The earth pressure coefficients are function of the effective stress friction angle ϕ'. For the simple case of a Rankine earth pressure with a horizontal backfill and no friction between the soil and the wall, the earth pressure coefficients can be estimated as follows:

$$K_a = \frac{1-\sin\varphi'}{1+\sin\varphi'} \quad (4)$$

$$K_p = \frac{1+\sin\varphi'}{1-\sin\varphi'} \quad (5)$$

$$K_o = (1-\sin\varphi')OCR^{\sin\varphi'} \quad (6)$$

Where OCR is the Over-Consolidation Ratio. The Canadian Foundation Engineering Manual (2006) provides a recommendation of using an earth pressure coefficient of 1 for rigid walls retaining swelling soils. NAVFAC DM7-02 recommends

DOI: 10.4417/IJGCH-08-04-01

using K_o to calculate the earth pressure with due consideration to potential poor drainage conditions, swelling, and frost action. NAVFAC further comments that the active earth pressure may be inadequate even for yielding walls, that the swelling pressure may be evaluated based on laboratory tests and that the wall may have to be designed to withstand swelling pressures. Hong et al. (2010) considered three profiles: a passive earth pressure profile, a swelling pressure profile, and an at rest earth pressure profile. They suggest using the passive earth pressure from the ground surface to the point where it intersects the swelling pressure profile, then following the swelling pressure profile until it intersects the at rest earth pressure profile, then switching to the at rest earth pressure profile below that point. As will be seen later, this recommendation, although based on sound principles, may be very conservative. Brown (2013) recommends using the active earth pressure of the fully softened drained shear strength of the retained soil. All these recommendations are very different; thus the need for this article.

SWELL PRESSURE PREDICTIONS

Because the swell pressure plays an important role in the selection of the horizontal pressure for walls retaining swelling soils, various equations to predict the swell pressure based on commonly measured soil properties are reviewed here. The goal is to recommend the most accurate equation by comparing predicted and measured values of the swell pressure ps. The following equations were identified.

Komornik and David (1969)

$$\log p_s = -2.132 + 0.0208LL + 0.000665\gamma_d - 0.0269\mathrm{w} \tag{7}$$

where ps is in kg/cm2, LL is the liquid limit in percent, γd is the total unit weight in kg/m3, and w is the water content in percent. This equation is based on 125 data records.

Nayak and Kristensen (1971)

$$p_s = 3.5817 \times 10^{-2} PI^{1.12} \frac{C^2}{w2} + 3.7912 \tag{8}$$

where p_s is in psi, PI is the plasticity index in percent, and C is the clay fraction in percent. This equation is based on 18 data records.

Schneider and Poor (1974)

$$\log p_s = -0.1234\mathrm{w} + 0.0316PI + 1.896 \tag{9}$$

where p_s is in tsf. This equation is based on 61 data records.

Komornik and David (1969)

$$\log p_s = -2.89 - 7.00\mathrm{w} + 6.65C \tag{10}$$

where p_s is in kg/cm^2. This equation is based on 10 data records.

The equations above are empirical and calibrated against databases of measured swell pressures. By combining all the data records associated with these equations and further searching for swell pressure data in the open literature, a database of 239

DOI: 10.4417/IJGCH-08-04-01

data records of measured swell pressures and associated basic soil properties was assembled. Each equation could then be evaluated against this expanded database. The scatter plots of predicted versus measured swell pressures on logarithmic scales using the expanded database for each equation is shown in Figure 1. In each plot, less than the total number of data record (239) is used because each data record did not possess all the data necessary for each equation being evaluated. A measure of the scatter was obtained by forming the ratio of the predicted over measured swell pressure ($P_{s,pred}/P_{s,meas}$) and calculating the mean μ and standard deviation σ of that ratio according to the normal distribution equations. The values of μ and σ for each equation are shown on each scatter plot. In addition to these scatter plots, another plot was created by using the average of the four predictions. This scatter plot is shown on Figure 2; it indicates that the average of the four equations gives a superior prediction to the individual ones since it gives an improved mean and standard deviation of the predicted over measured swell pressure ratio.

Note also that p_s is the swell pressure obtained in the laboratory by preventing any swelling after inundation also known as the no-volume change swell pressure. Allowing some volume change during the test will reduce the value of ps. Furthermore, the initial water content of the soil will have an impact on p_s as shown in the equations. In essence, a relatively dry soil behind a very rigid wall is likely to develop much higher horizontal pressures than a relatively wet soil behind a flexible wall. Thus, these factors need to be considered.

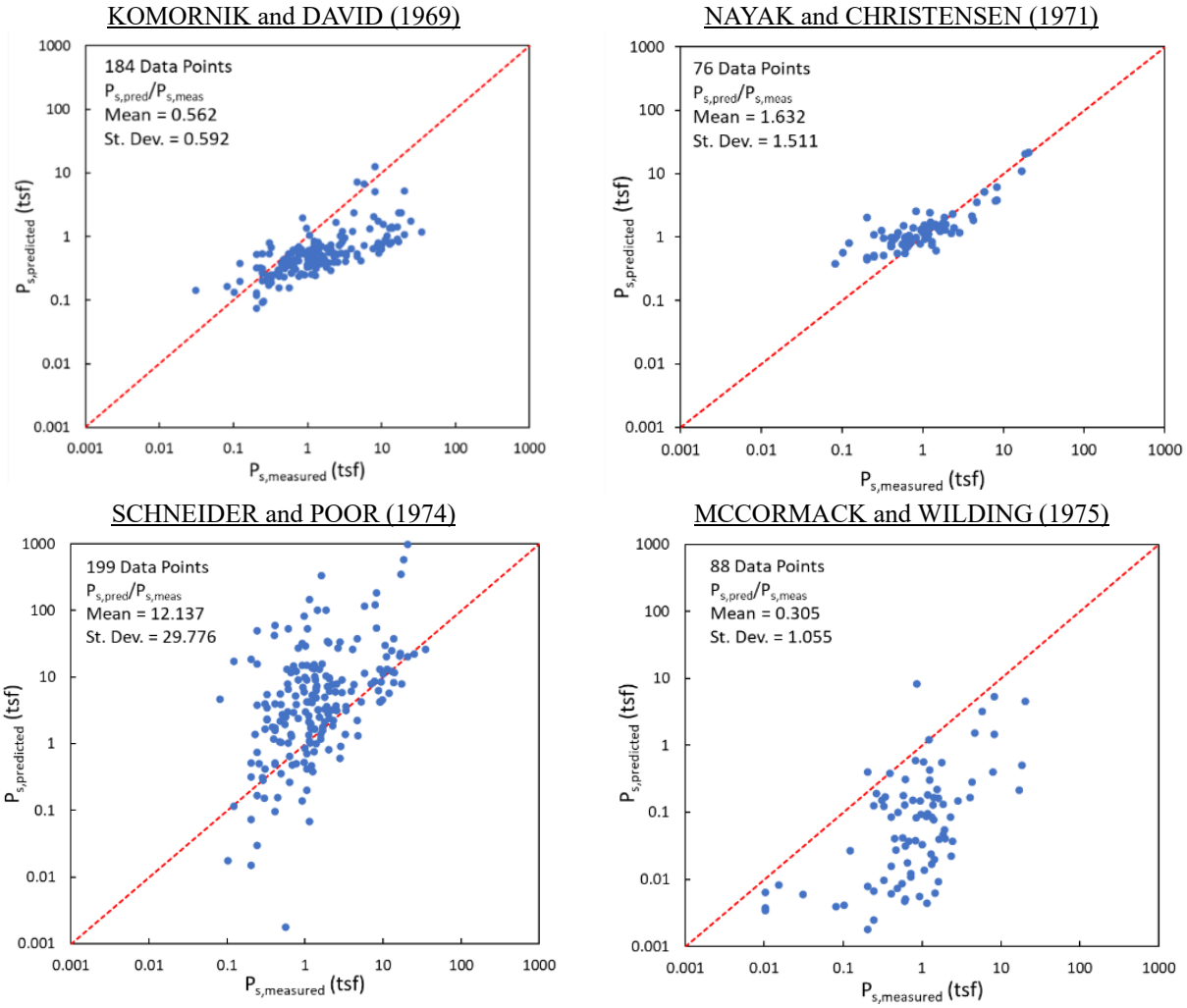

Figure 1. *Predicted versus measured swell pressure by four equations.*

DOI: 10.4417/IJGCH-08-04-01

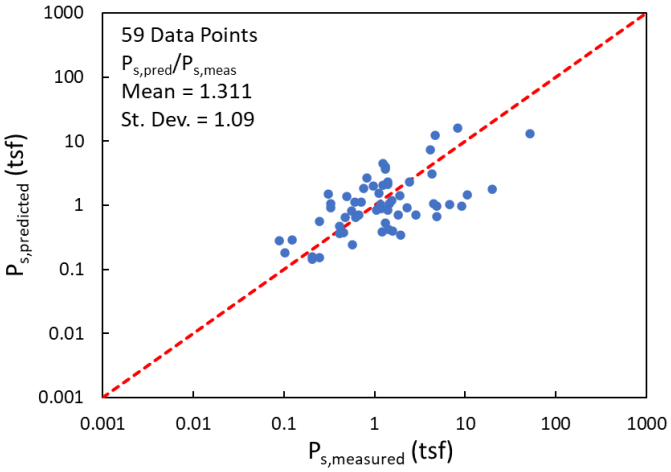

Figure 2. *Predicted versus measured swell pressure by the average of the four equations.*

SOME PREVIOUS STUDIES ON WALLS RETAINING SWELLING SOILS

There are only a few previous studies related to walls retaining swelling soils. In the laboratory, researchers have worked on estimating lateral swell pressures in instrumented consolidometers and special triaxial tests (Komornik and Zeitlen, 1965; Ofer ,1981). Thomas et al. (2009) suggest that the wall pressure distribution in the case of swelling soils should include the swell pressure and propose a triangular distribution increasing with depth. They show that the factor of safety against sliding decreases significantly when including the swell pressure. They recommend a design limit to the swell pressure to satisfy a reasonable factor of safety against sliding and add some recommendations to achieve such a limit. Bilgin and Mansour (2013) performed a parametric design study of a fictitious anchored wall and showed that including the swell pressure in the design has a drastic impact on the embedment depth, on the anchor force, and on the maximum bending moment. None of these studies address the issue of waterfront-time propagation into the soil behind the wall which has a significant impact on the swell pressure to be considered in design. That is considered in this study.

ANALYSIS OF CASE HISTORIES OF WALLS RETAINING SWELLING SOILS

Table 1 shows the case histories of walls retaining swelling soils selected from the literature. The basic criterion was to find walls retaining fine-grained soils with a plasticity index higher than 20%. Only 3 relevant case histories or large-scale laboratory experiments were found (Table 1). All soils are high plasticity clays and silts with a CH (high plasticity clay) or MH (high plasticity silt) USCS classification. Some walls are unyielding, and some are allowed to move. The retained soils are artificially inundated by ponding or by keeping boreholes full of water. The period of observation and inundation varies from two months to two years. The pressure distributions obtained from the case histories are shown in Figures 3, 4, and 5. The case histories are analyzed one by one.

Katti et al. (1983) wall. This wall experiment is also described in Joshi and Katti (1980) and in Kate and Katti (1980). This is a large-scale experimental bottom-up wall at the Indian Institute of Technology in India, which is 3.0 m high, 1.65 m wide, and 1.2 m long (Figure 3). As such it represents a fairly narrow bin filled with soil. The backfill is known locally as “black cotton clay”; it has a liquid limit of 71.4%, a plasticity index of 29.4%, a shrinkage limit of 10.4%, 55% clay fraction, and classifies as an MH. The backfill was compacted in lifts at a water content of 7% and a total unit weight of 13.1 kN/m3; this unit weight seems quite low. Direct shear tests gave c’ = 10 kPa and ϕ’ = 21o. Vane tests gave an undrained shear strength varying from 6 kPa at 0.1 m depth increasing to 59 kPa at 2.5 m depth averaging 50 kPa from 1 m down. The swell pressure was determined to be 225 kPa for the oven dry soil. Water to foster the swelling of the fine-grained soil was provided to the backfill for 67 days through the base, through the side in the back of the backfill and by ponding on the soil surface at the

DOI: 10.4417/IJGCH-08-04-01

top. The water content after inundation increased to 55% at the surface with an average of 40% below 1 m depth. The pressure on the wall due to inundation for 2 months is much higher than that given by a K_o or even a K_p distribution (Figure 3). Indeed, the pressure reaches 250 kPa at a depth of 2 m, which is close to the swelling pressure. This is thought to be due to the low water content at which the soil was compacted, giving it significant swell potential, and to the narrow bin effect which generates significant confinement; this confinement allows for the development of the full no-volume change swell pressure similar to the laboratory swell pressure.

Clayton et al. (1991) wall. This is a large-scale bottom-up experimental wall at the Transport and Road Research Laboratory in the UK which is 3 m high, 5 m wide, and 6 m long (Figure 4). A flexible metal wall is on one side of the container and a rigid 1 m thick concrete wall is on the other side. The backfill was London clay which had a liquid limit of 78%, a plasticity index of 49%, 60% clay fraction, and classifies as CH. It was compacted in lifts at a water content of 28.5% and a total unit weight of 18.1 kN/m3. Unconsolidated undrained triaxial tests gave an undrained shear strength averaging 125 kPa. Consolidated undrained triaxial tests with pore pressure measurements gave c' = 15 kPa and ϕ' = 19o. The laboratory one-dimensional swell pressure p_s was 375 kPa. Forced inundation was induced by 2 m deep saturated boreholes (Figure 4) for 623 days. The maximum pressure on the walls was observed after 210 days of inundation; at that point the pressure distribution was closer to being constant with depth than triangular and had values ranging from 21-26% of p_s (Figure 4). This small fraction of p_s is attributed to the fact that, while p_s is measured with unyielding confinement in the consolidometer, the ground surface of the wall backfill can swell vertically. This reduces the horizontal swell pressure on the wall to an upper limit equal to the passive earth pressure. In Figure 4, in addition to the measured pressure, several calculated profiles using Eqs. 2 and 3 are shown. They are the total at rest pressure and the total passive pressure. For each one, two assumptions are made: a full hydrostatic pressure starting at the ground surface and zero water stress in the soil mass. The passive pressure profiles match the long-term profiles best. Note that the pressure on the wall decreased from 210 days to 692 days while inundation continued; this is likely due to softening of the London clay.

Brown (2013) wall. This is a full-scale outdoor top down retaining wall project in Manor, Texas, conducted by the University of Texas at Austin (Figure 5). This research wall was built by constructing a row of 25 drilled shafts 0.61 m in diameter, 10.7 m in length, and with a center to center spacing of 0.76 m. Once the drilled shafts were constructed, one side of the row of drilled shafts was excavated down to 4.6 m, leaving 6.1 m of embedment below excavation. The soil behind the wall was a high plasticity clay with a liquid limit averaging 80% within the excavated soil depth and a corresponding plasticity index of more than 40%, leading to a USCS classification of CH. The average water content within the retained depth averaged 25% before excavation and inundation, and the average unit weight was 19.2 kN/m3. The undrained shear strength within the retained depth averaged 72 kPa. The effective stress cohesion and the effective stress friction angle were 55 kPa and 17.7o respectively for the peak strength, and 6.5 kPa and 24o for the fully softened strength. The hydraulic conductivity was measured to be between 1 x 10-14 and 3 x 10-14 m/s. The no-volume change swell pressure was 57 kPa at a depth of 1.5 m, and 182 kPa at a depth of 4.6 m; therefore, the swell pressure increased approximately linearly with depth while being less than the passive pressure. Many more details on the soil properties can be found in Ellis (2011).

The wall was instrumented primarily with inclinometer tubes in the drilled shafts to obtain the wall deflection profile, and strain gages on the reinforcing bars of the drilled shafts to obtain the bending moment profile in the drilled shafts upon excavation. The top of the wall deflected 25 mm toward the excavation during the 4.6 m excavation, after which it was subjected to the natural weather for 580 days and deflected an additional 19.5 mm. Then the back of the wall was inundated for 60 days and the wall deflected an additional 58.3 mm. Then after 210 days without inundation and no appreciable wall movement, the back of the wall was inundated again for 120 days, during which the top of the wall deflected an additional 30 mm. In total, the top of the wall moved 132.8 mm or 2.9% of the retained height. The pressure on the wall was not measured but inferred by differentiation from the measured deflection and moment profiles; the best fit inferred pressure profile leads to pressures much smaller than the swell pressures. Based on all measurements and numerical simulations,

DOI: 10.4417/IJGCH-08-04-01

Brown (2013) recommends designing such walls for the effective active earth pressure using the fully softened effective strength parameters plus the hydrostatic pressure of the maximum realistic water table height.

Table 1. *List of case histories of walls retaining swelling soils.*

No.	Authors and date	Soil type	Wall type	Wall dimensions and water table (WT)	Comments
1	Katti et al. (1983)	MH, PI_{ave} = 29.4%, p_s = 220 kPa, w = 7% before test, γ_{ave} = 13.1 kN/m^3, c' = 10 kPa, ϕ' = 21°, s_u = 50 kPa	Bottom up, unyielding	3.0 m high, 1.65 m wide, 1.2 m long, no WT	Compacted soil, inundation from top, side and bottom of tank for 67 days
2	Clayton et al. (1991)	CH, PI = 49%, p_s = 375 kPa, w = 28.5% before test, γ = 18.1 kN/m^3, c' = 15 kPa, ϕ' = 19°	Bottom up, unyielding, yielding	3 m high, 5 m wide, 6 m long, no WT	Compacted soil, saturated with 2 m deep sand drains for 623 days
3	Brown et al. (2013)	CH, PI > 40%, p_s = 27.2 to 181.9 kPa, w_{ave} = 25% before test, c'_{peak} = 55 kPa, ϕ'_{peak} = 17.7°, $c'_{softened}$ = 6.5 kPa, $\phi'_{softened}$ = 24° , $s_{u\ ave}$ = 72 kPa, k = 10^{-14} m/s	Top down cantilever wall, row of drilled shafts	Drilled shaft 0.61 m diameter, 0.762 m center to center, 4.6 m excavation, 6.1 m embedment	Water table at 2.44 m depth. Inundated for 6 months in total

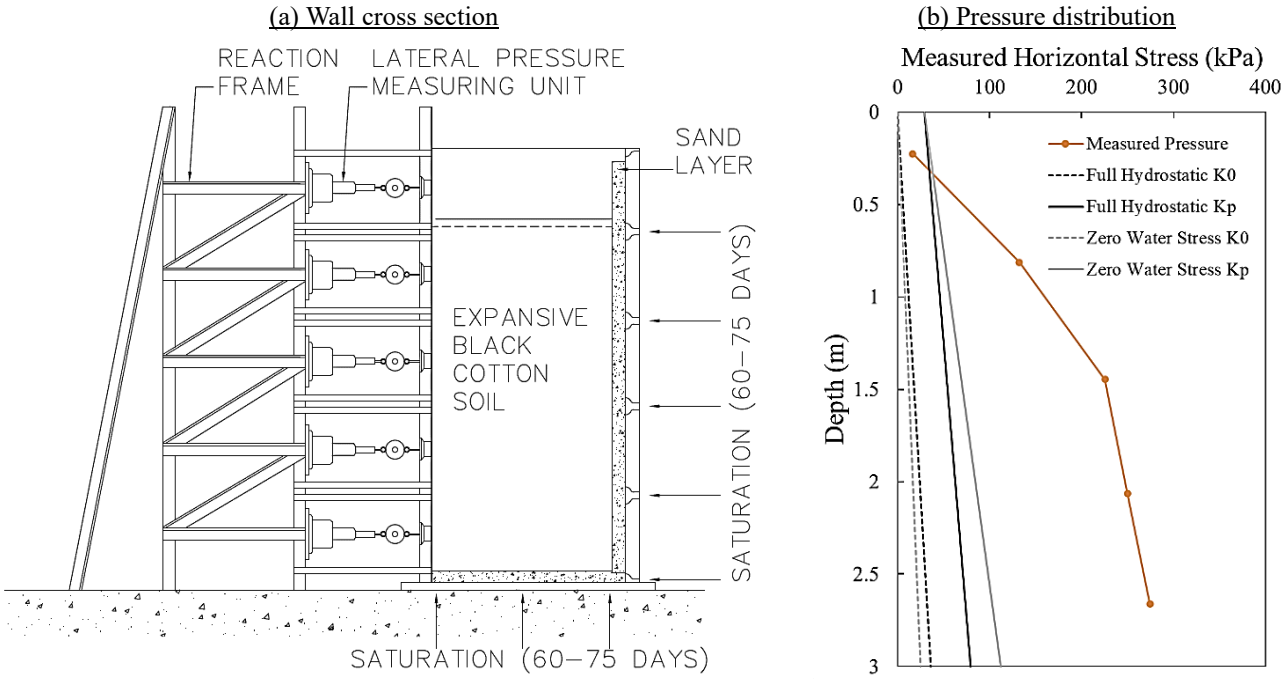

Figure 3. *Measured pressure distribution for Katti et al. (1983) wall: (a) wall cross section, (b) pressure distribution (after Katti et al., 1983).*

DOI: 10.4417/IJGCH-08-04-01

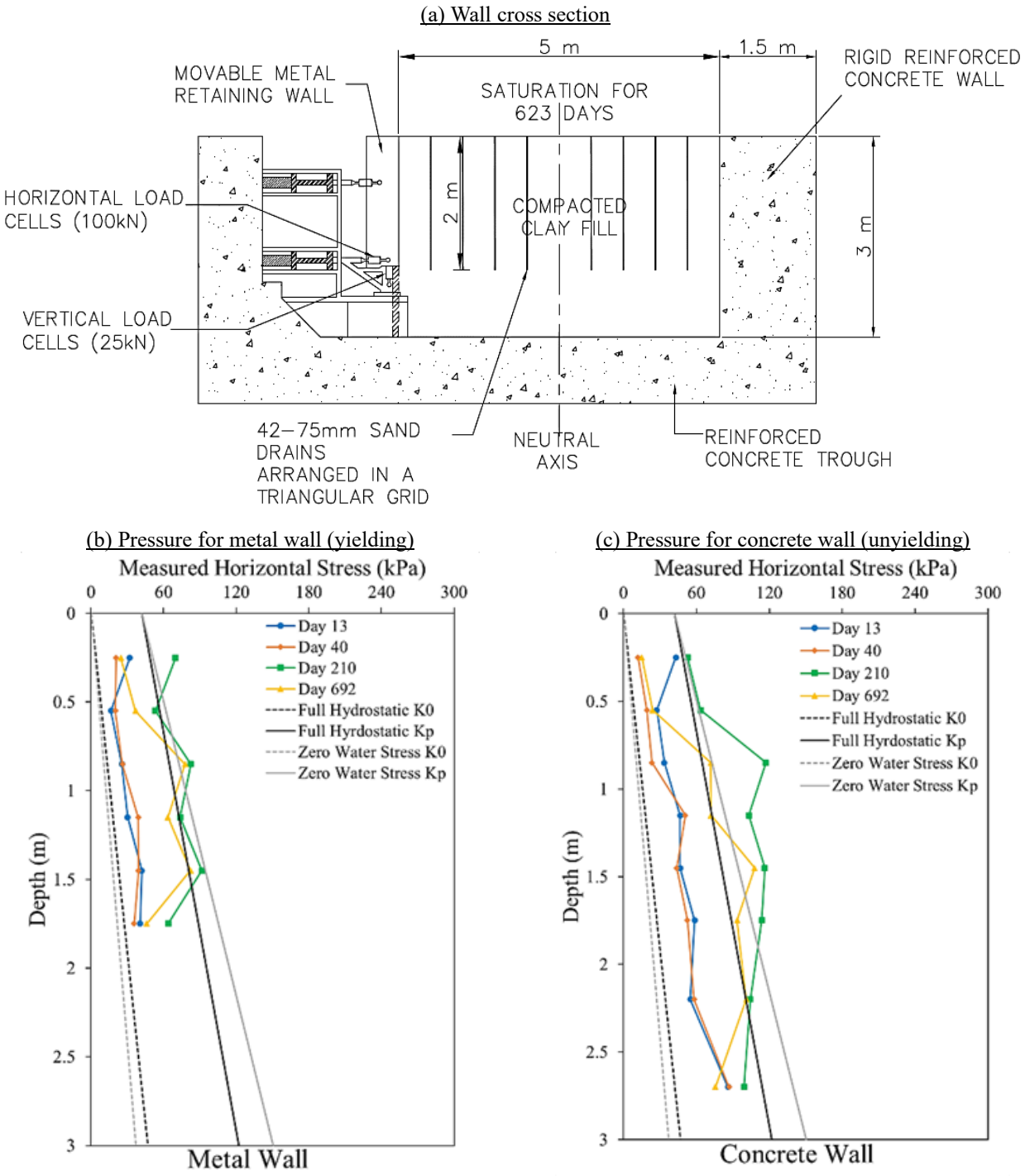

Figure 4. *Measured pressure distribution for Clayton et al. (1991) wall: (a) wall cross section, (b) pressure for metal wall (yielding), (c) pressure for concrete wall (unyielding) (after Clayton et al., 1991).*

DOI: 10.4417/IJGCH-08-04-01

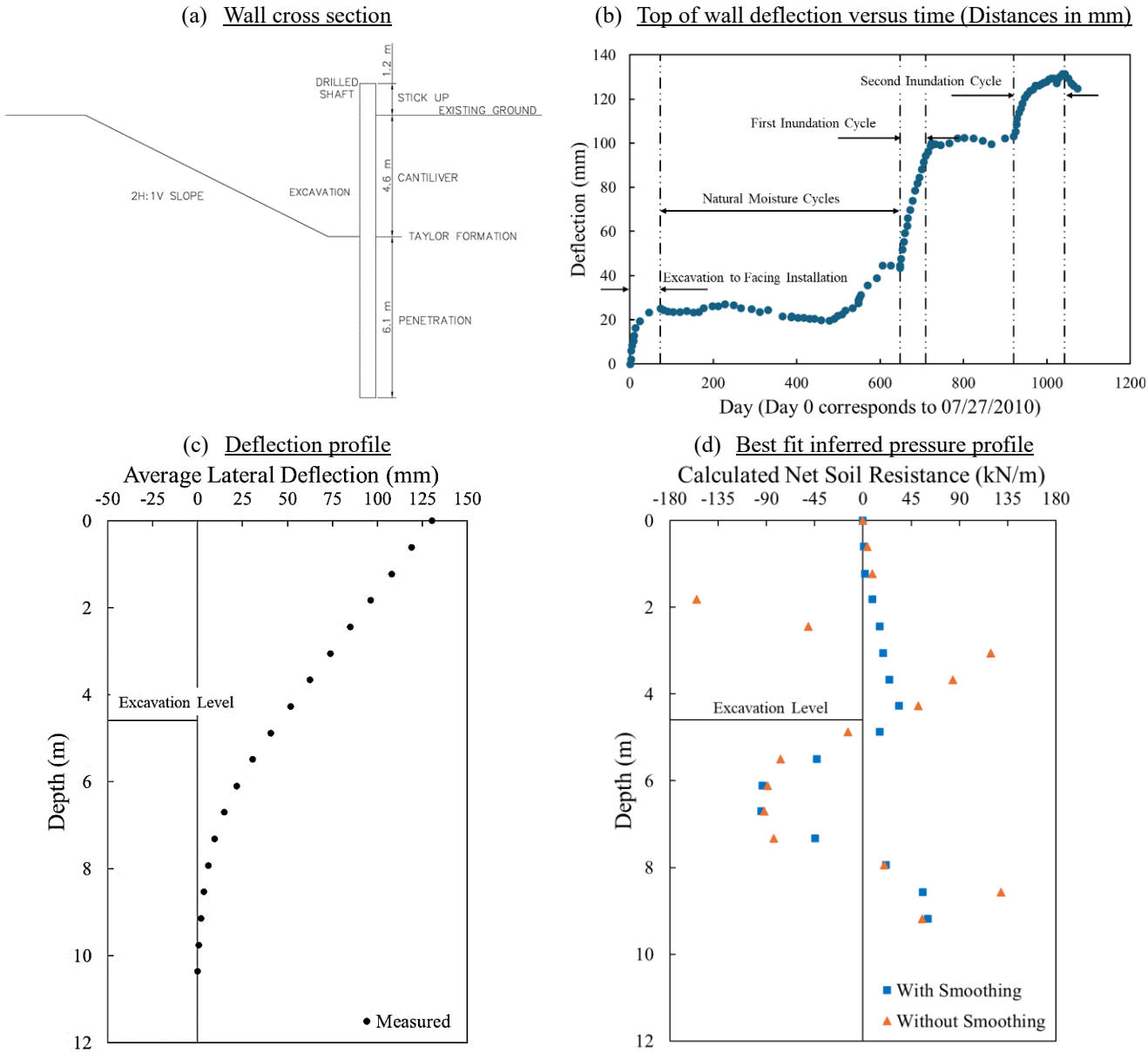

Figure 5. *Measured pressure distribution for Brown (2013) wall: (a) wall cross section, (b) top of wall deflection versus time, (c) Deflection profile, (d) best fit inferred pressure profile (after Brown, 2013).*

NUMERICAL SIMULATIONS OF WALLS RETAINING SWELLING SOILS

To better understand the influence of various key factors on the pressure against walls retaining swelling soils and to complement the case histories studied, a series of simulations were undertaken using the fully coupled finite element program CODE_BRIGHT (Olivera et al., 1996, CODE_BRIGHT Manual 2023). To represent the mechanical behavior of swelling soils, a modified version of the Barcelona Basic Model (BBM) (Alonso et al., 1990) was adopted. A brief model description is presented in the Appendix, and more details can be found in Sanchez et al. (2012). The Appendix also presents the hydraulic models used in this research. The next section describes the modeling of swelling pressure tests (used to estimate the model parameters) and the simulation of retaining wall cases.

DOI: 10.4417/IJGCH-08-04-01

Simulation of Swell Test in Consolidometer

The behavior of the sample in the consolidometer for a constant volume swell test was simulated assuming a 2D Y-axisymmetric geometry. Furthermore, considering the mechanical and flow conditions in a standard oedometer cell, only the top half of the sample height was modeled. Figure 6 shows the 31.5 mm diameter and 9 mm high mesh adopted in this study to represent a standard 63 mm x 18mm consolidation sample. An initial suction s_0 = 12MPa was assumed. The boundary conditions prevented any movement in all directions. Water inflow at the top of the mesh was imposed by establishing a zero suction boundary condition. Table 2 lists the BBM parameters adopted in this work. These parameters were obtained by matching the swell pressure of 350 kPa, measured in an experiment conducted on a local natural shrink/swell soil (Figure 7). The main clay properties are also listed in Table 2.

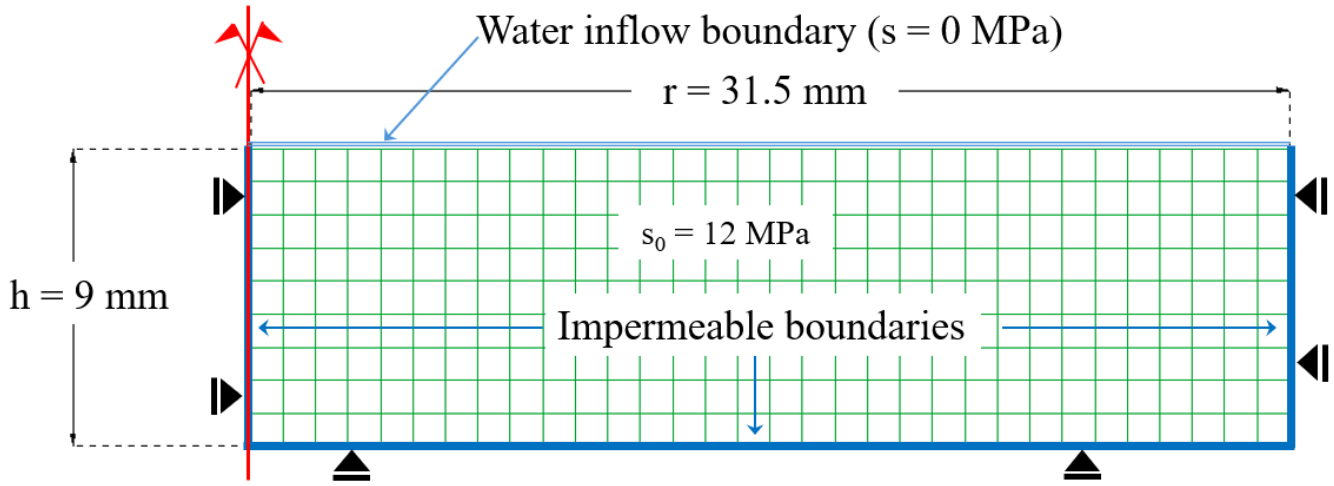

Figure 6. *Mesh dimensions and boundary conditions for the consolidometer swell test.*

Table 2. *Soil BBM model parameters and clay properties.*

κ_{i0}	κ_{s0}	K_{min} (MPa)	ν	α_{ss}	α_{il}	α_i	α_{sp}	p_{ref} (MPa)
0.01	0.02	10	0.3	-0.05	0.0	0.0	0.0	0.01

λ	r	β (1/MPa)	k	p_{s0} (MPa)
0.11	0.7	12.5	0.03	0.01

p_c (MPa)	M	α	e_0	p_{0*} (MPa)
0.1	1.03	0.6	0.95	0.2

P_0 (MPa)	λ	k_0 (m^2)	φ_0	b
1	0.26	4.917×10^{-17}	0.465	65

Liquid limit (%)	65
Plastic limit (%)	23
USCS classification	CH
Dry unit weight (kN/m^3)	13.53
Initial water content (%)	14
Initial degree of saturation (%)	41
Saturated unit weight (kN/m^3)	17.47
Initial suction (MPa)	12
Permeability (m/s)	4.82×10^{-11}
Friction angle (º)	26
Cohesion (kPa)	10
Overconsolidation ratio	2

DOI: 10.4417/IJGCH-08-04-01

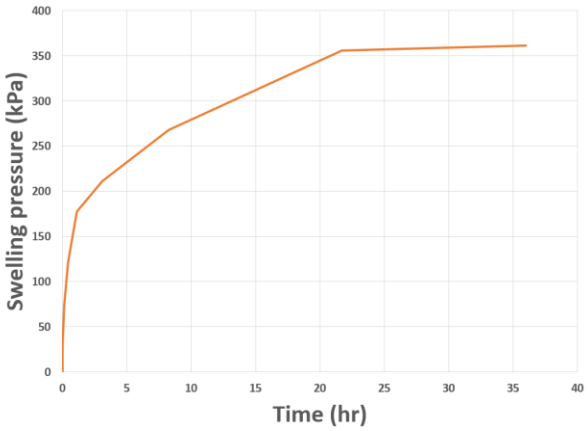

Figure 7. *Constant volume consolidometer swell test: vertical pressure vs. time from the experiment.*

The horizontal stress on the side of the consolidometer is plotted in Figure 8, along with the horizontal stress after removing the vertical constraint at the top of the sample (free swell test). As expected, the horizontal stress is much lower for the free swell test than for the no-volume change experiment. A free swell top boundary is much like a retaining wall boundary condition where the top boundary is allowed to move/swell vertically. The reason the horizontal pressure on the vertical wall of the consolidometer ring in the free swell test is much lower than the swell pressure in the no-volume change swell test is that it is limited by the passive earth pressure of the soil, which is quite small for an 18 mm high consolidometer "retaining wall" ring. Indeed, in this case, the passive wedge is able to form and move upward behind the steel ring wall.

For the parameters and conditions considered in this work, the no-volume change model predicts a lateral stress slightly higher than the measured swelling pressure of 350 kPa. The literature reports lateral stresses both higher (e.g., Fourie, 1989; Liu et al., 2021) and lower than the vertical stress (e.g., Zhang et al., 2020). It is also noted that the distribution of lateral stresses is not uniform along the height of the sample. This is because we model this test as a boundary value problem. It is worth highlighting that the adopted bulk modulus (i.e., equation A12 in the appendix) is not constant but depends on the mean stress and void ratio. The clay is more compressible at the beginning of hydration than at the end because of the increase in p during wetting, which induces a non-uniform distribution of void ratios and stress.

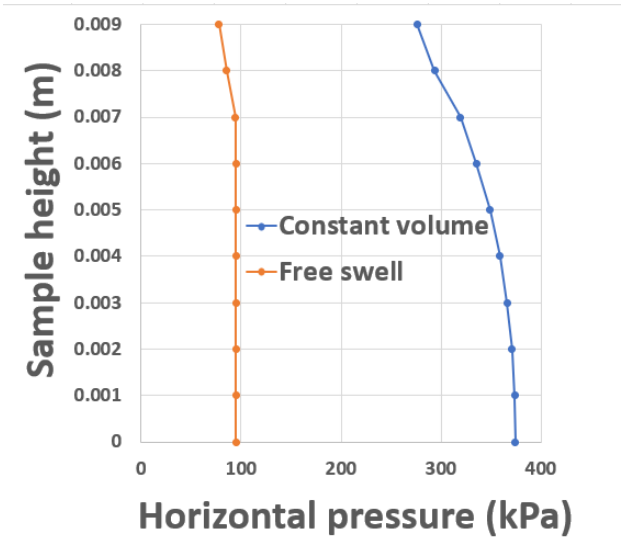

Figure 8. *Constant volume consolidometer swell test: lateral pressure on vertical wall from the simulation.*

DOI: 10.4417/IJGCH-08-04-01

Retaining Wall Simulation

Maximum pressure distribution

To study the development of the pressure behind a wall retaining a swelling soil subjected to wetting, a generic retaining wall was adopted with a plane strain condition. The same swelling soil discussed in the swell test of the previous section was adopted (i.e., same BBM parameters). The wall was 5 m high, and the outer boundaries were as shown in Figure 9. All boundaries were prevented from moving, including the wall, except for the top boundary which was free to move. A ground water level was set 10 m below the bottom of the wall. The initial suction in the soil was set at 12 MPa. The simulation was performed by keeping the free surface at the top of the wall inundated (suction = 0).

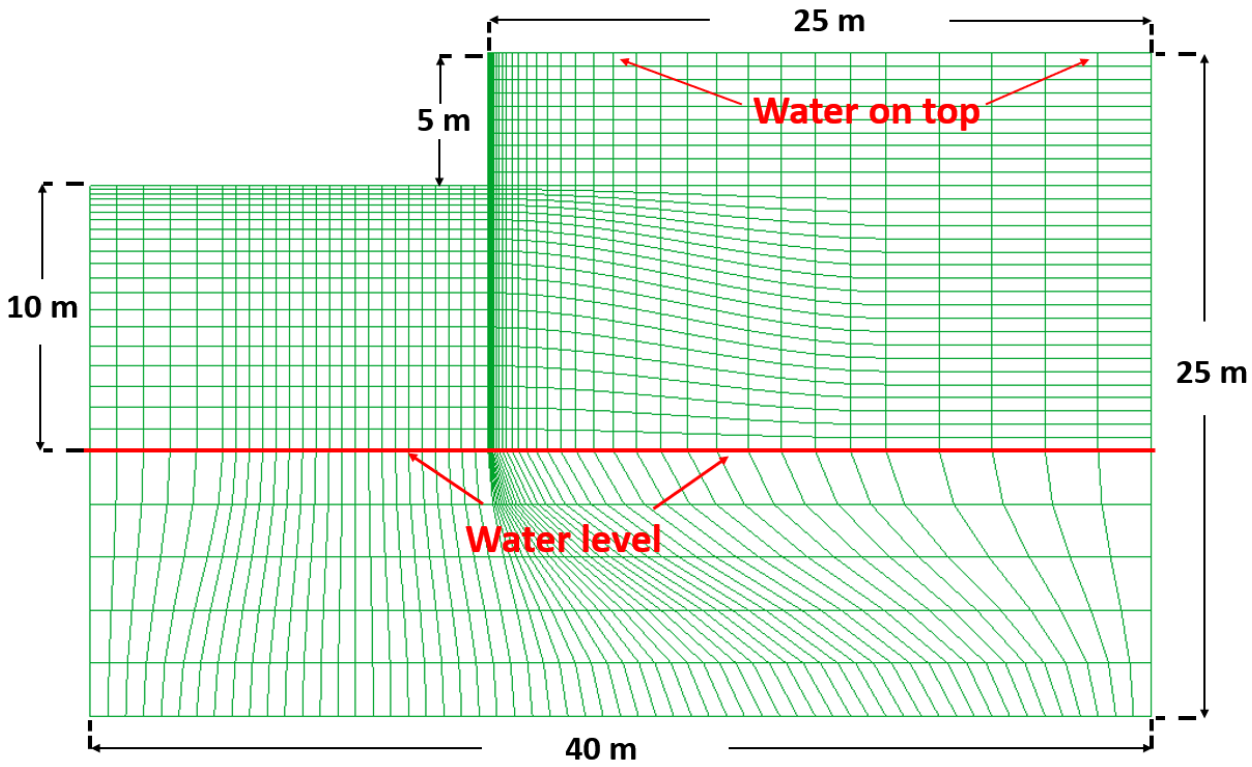

Figure 9. *Boundaries for wall simulation.*

The output of the simulations was the pressure profile on the wall as a function of the time required for the wetting front to propagate downward in the soil mass. Figure 10 shows the pressure profiles as a function of time. These pressure profiles are bounded by two earth pressure profiles. The lower bound is the at rest earth pressure profile and the upper bound is the passive earth pressure profile as the swell pressure cannot be larger than the passive earth pressure. The horizontal at rest earth pressure σ_{oh} profile is calculated according to Eq. 3 with u_w equal to zero as the suction decreases to zero because of ponding, and with Ko expressed as follows:

$$K_o = (1 - sin\,\varphi\,')OCR^{sin\,\varphi'} = (1 - sin\,2\,6) \times 2^{sin\,26} = 0.761 \quad (11)$$

At the bottom of the 5 m high wall, this gives (Figure 10):

$$\sigma_{oh} = 0.761 \times (13.53 \times (1 + 0.14) \times 5) = 58.7kPa \quad (12)$$

DOI: 10.4417/IJGCH-08-04-01

The horizontal passive earth pressure σ_{ph} profile is calculated according to Eq. 2 with u_w equal to zero as the suction decreases to zero because of ponding, and with K_p expressed as follows:

$$K_p = \frac{1+\sin\varphi'}{1-\sin\varphi'} = \frac{1+\sin 26}{1-\sin 26} = 2.561 \quad (13)$$

At the bottom of the 5 m high wall, this gives (Figure 10):

$$\sigma_{ph} = 2.561 \times (17.47 \times 5) + 2 \times 10\sqrt{2.561} = 255.7kPa \quad (14)$$

Figure 10 shows that the pressure against the wall increases as the wet front propagates downward and the soil swells. The maximum pressure is limited by the passive earth pressure and decreases to join the at rest earth pressure below the waterfront. After 5 days, the highest pressure is 1 m deep and equal to 75 kPa, but after 40 days the pressure profile approaches the passive pressure profile. In this case, the swell pressure is not reached, since it is 350 kPa, while the maximum passive pressure is 255.7 kPa.

Figure 11 shows the same case, except with a swell pressure of 150 kPa. In this case, the bottom part of the pressure profile does not reach the passive earth pressure and is limited by the swell pressure equal to 150 kPa. Figure 12 shows the same case, except with a swell pressure of 81 kPa. Again, in this case, the bottom part of the pressure profile is limited by the swell pressure equal to 81 kPa after 40 days of inundation. These cases show that the maximum pressure that can develop against a wall retaining a swelling soil is as shown in Figure 13. This figure can serve as a guide for the maximum pressure that can be exerted against a wall retaining a swelling soil.

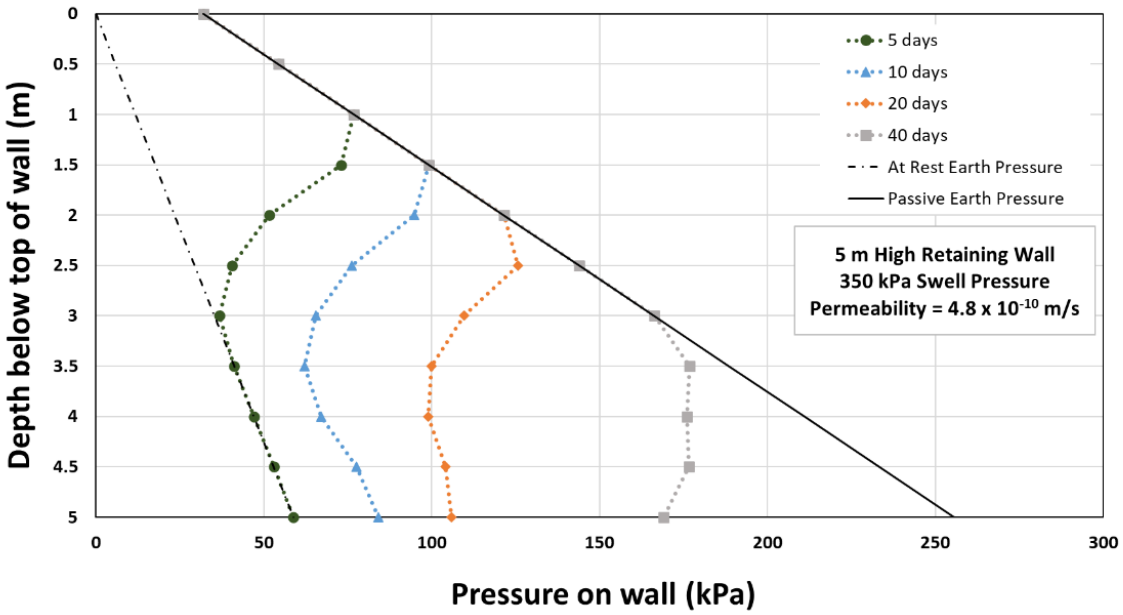

Figure 10. *Pressure on 5 m wall with 350 kPa swell pressure and 4.82x10-10 m/s permeability as a function of time.*

DOI: 10.4417/IJGCH-08-04-01

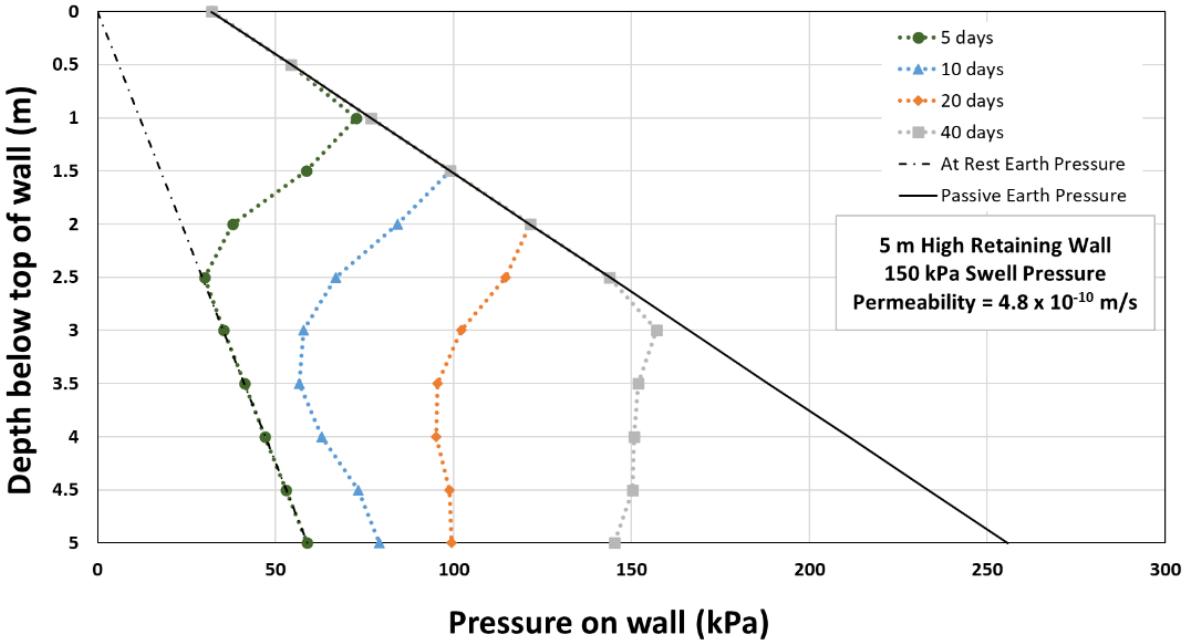

Figure 11. *Pressure on 5 m wall with 150 kPa swell pressure and 4.82x10-10 m/s permeability as a function of time.*

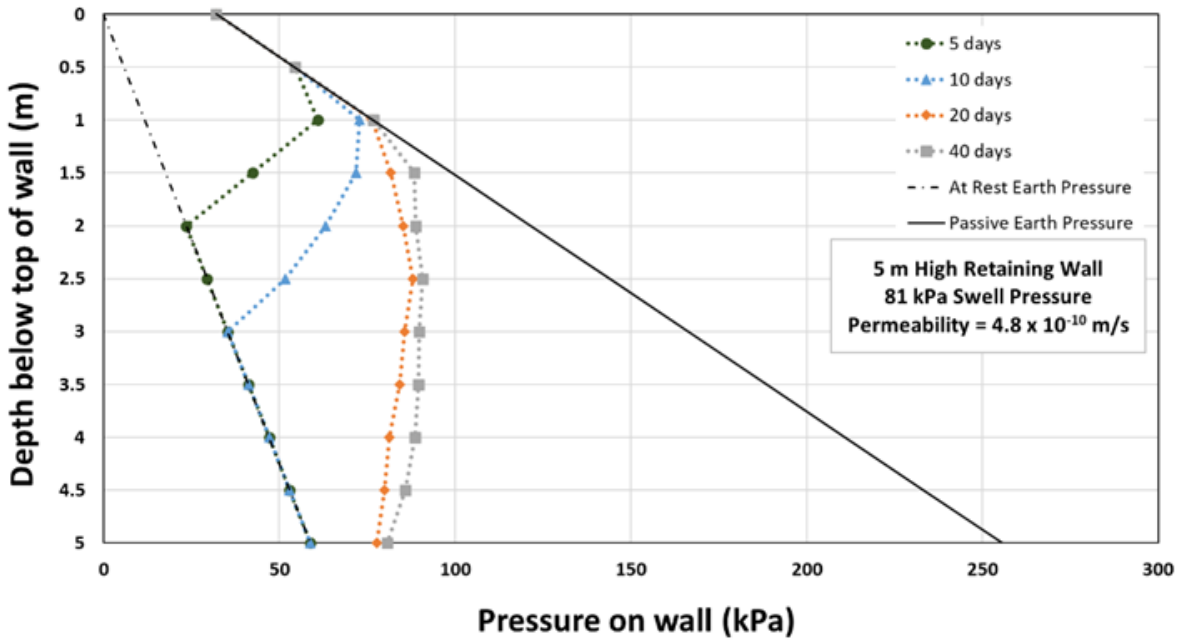

Figure 12. *Pressure on 5 m wall with 81 kPa swell pressure and 4.82x10-10 m/s permeability as a function of time.*

DOI: 10.4417/IJGCH-08-04-01

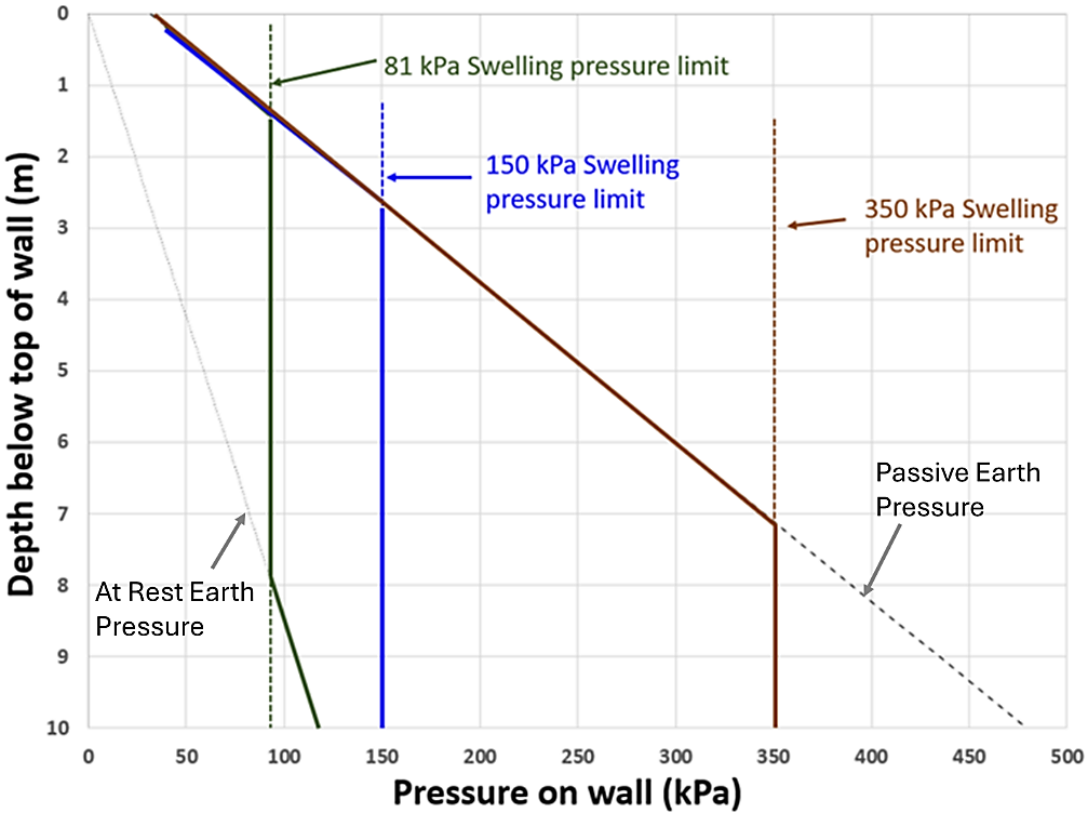

Figure 13. *Suggested maximum pressure distribution for walls retaining swelling soils.*

Pressure distribution versus time

The maximum pressure distribution of Figure 13 requires a long period of inundation which may not be realistic. As such, there is a need to develop a time-dependent pressure distribution behind such retaining walls. To regroup all the results of the simulations, a non-dimensional time factor β was defined as:

$$\beta = \frac{kt}{H} \tag{15}$$

where k (m/s) is the soil permeability or hydraulic conductivity, t (s) is the elapsed time after inundation starts, and H (m) is the wall height. For example, the time factor β for the 1 m deep point on Figure 10 would be:

$$\beta = \frac{4.82\times10^{-10}\times5\times24\times3600}{5} = 4.16\times10^{-5} \tag{16}$$

This time factor allowed for the regrouping of simulation results for different soil permeability, soil swelling pressures, and elapsed time. The recommendations are then shown in Figures 14a, 14b, 14c for a 2 m high, 5 m high, and 10 m high wall respectively. Note that these figures were generated for a high swelling pressure and thus the vertical swelling pressure lines represent limits to be applied to the pressure diagrams.

DOI: 10.4417/IJGCH-08-04-01

(a) 2 m HIGH WALL

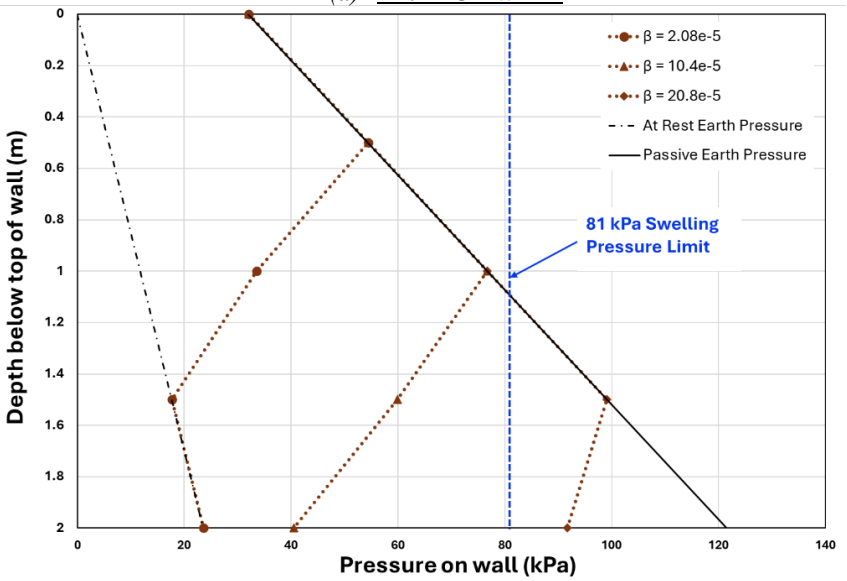

(b) 5 m HIGH WALL

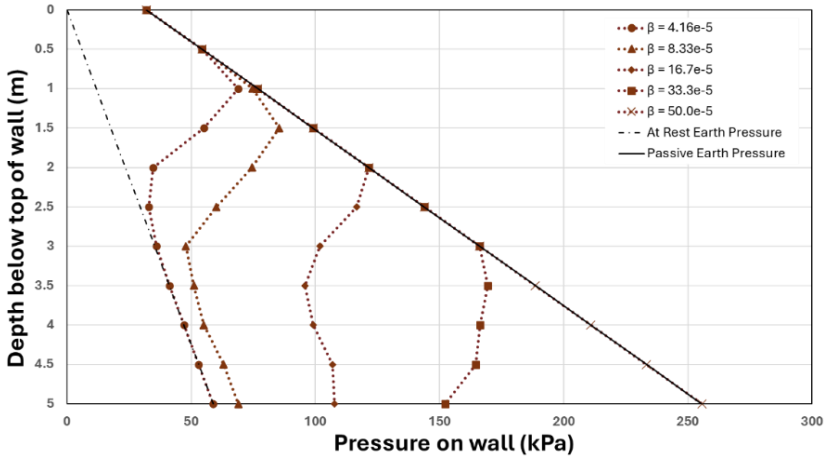

(c) 10 m HIGH WALL

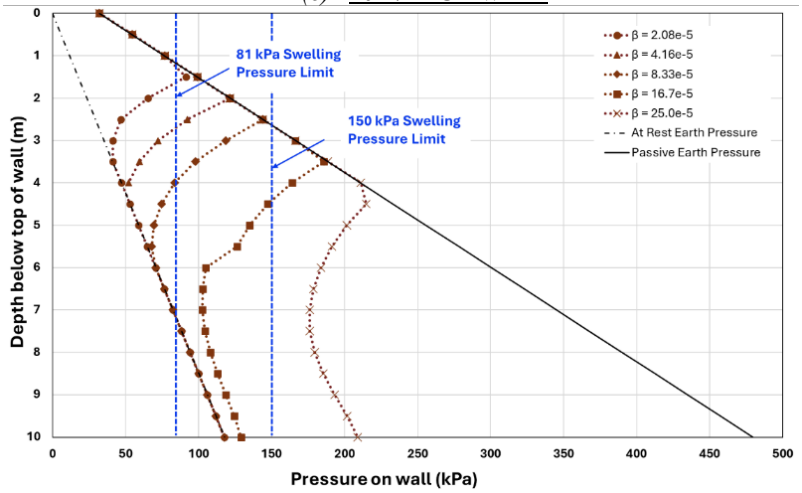

Figure 14. *Suggested time-dependent pressure distributions for walls retaining swelling soils.*

DOI: 10.4417/IJGCH-08-04-01

Influence of wall movement.

The 5 m high bottom-up wall was simulated after allowing for a 50 mm, a 15 mm, and a 0 mm (unyielding) horizontal movement respectively. As can be seen in Figure 15, the wall movement decreases the 10-day pressure distribution. However, the pressure distribution increases with time, as shown in Figure 16(a). A comparison between Figures 16(a) and 16(b) shows that, overall, the pressure on the wall moving 50 mm is anywhere from 30-50% less than the pressure on the unyielding wall.

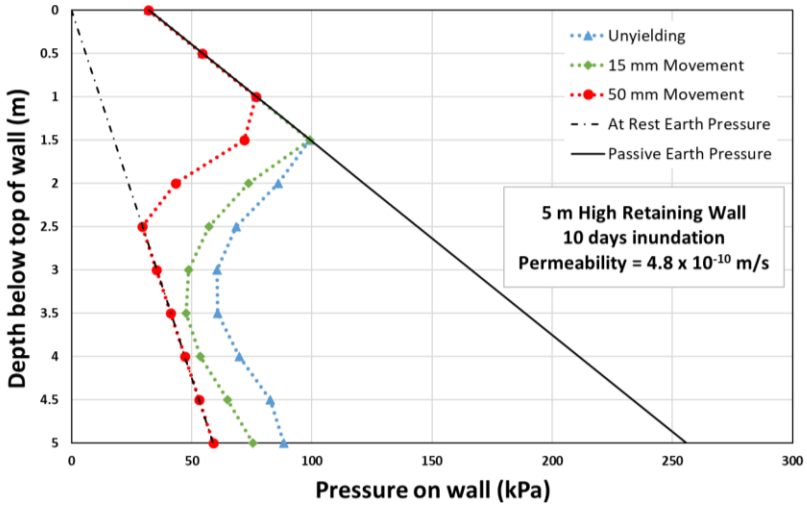

Figure 15. *Influence of wall movement on pressure against wall (after 10 days of inundation).*

(a) 5 m HIGH UNYIELDING WALL *(b) 5 m HIGH WALL MOVED 50 mm*

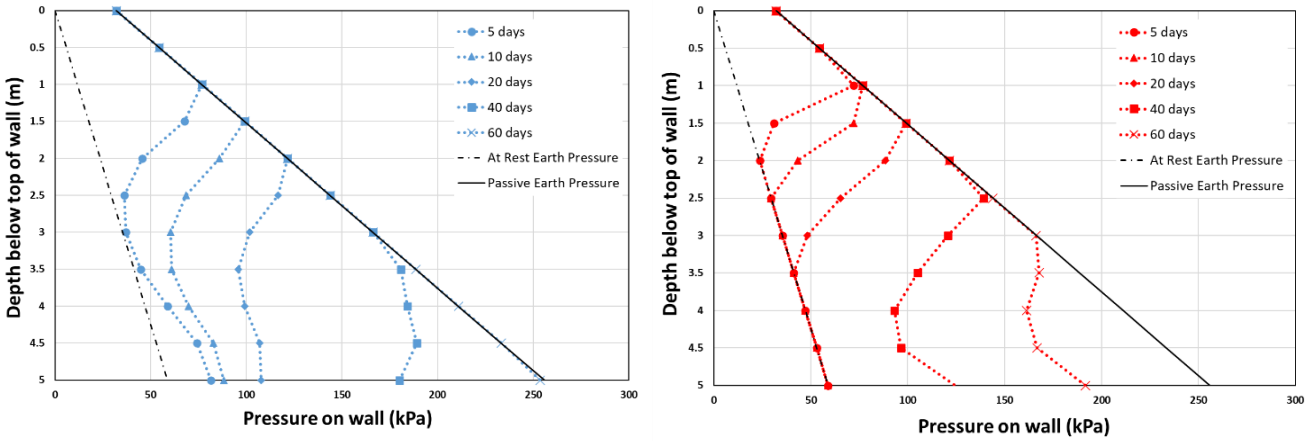

Figure 16. *Comparing (a) time-dependent pressure on unyielding wall and (b) time-dependent pressure on wall moving 50 mm.*

Comparison with case histories

Two wall case histories were then simulated to verify that the numerical simulation could match the measured pressures. The first case was Katty et al. (1983). The soil data given for that case history (Table 1) were used to develop the CODE_BRIGHT parameters. This process included matching the swelling pressure of 225 kPa. The simulations were performed until the inundation time of 67 days was reached. The results are shown in Figure 17 and indicate a good agreement between the simulated pressures and the measured pressures. Again, the pressure against the wall reached the swell pressure, and more,

DOI: 10.4417/IJGCH-08-04-01

because the bin effect provided by the narrow container (width over height ratio = 0.55) used in the experiment prevented the passive earth pressure wedge to develop and limit the pressure against the wall except at the very top of the bin.

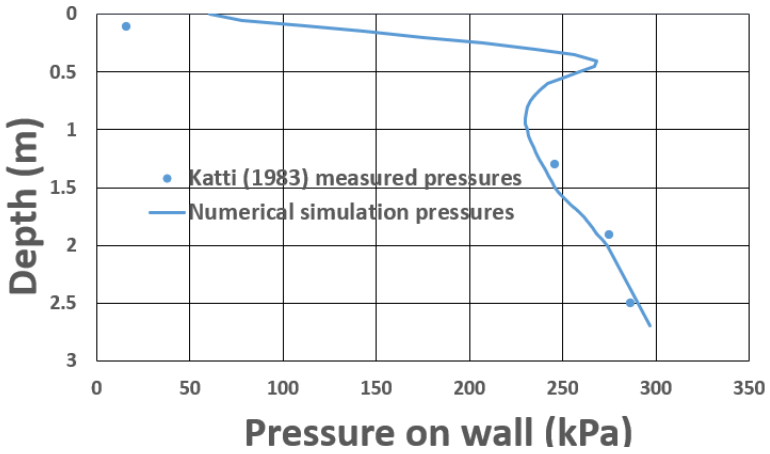

Figure 17. *Measured and simulation pressures on wall for Katti (1983) experiment.*

The second case was Clayton et al. (1991). The soil data given for that case history (Table 1) were used to develop the CODE_BRIGHT parameters. This process included matching the swelling pressure of 375 kPa. The simulations were performed until the inundation time of 692 days was reached. The results are shown in Figure 18 and indicate a reasonable agreement between the simulation pressures and the measured pressures. In this case, the container was much larger for its height (width over height ratio = 1.64) and allowed the earth pressure wedge to develop, thus limiting the pressure on the wall to the passive earth pressure and not the swell pressure.

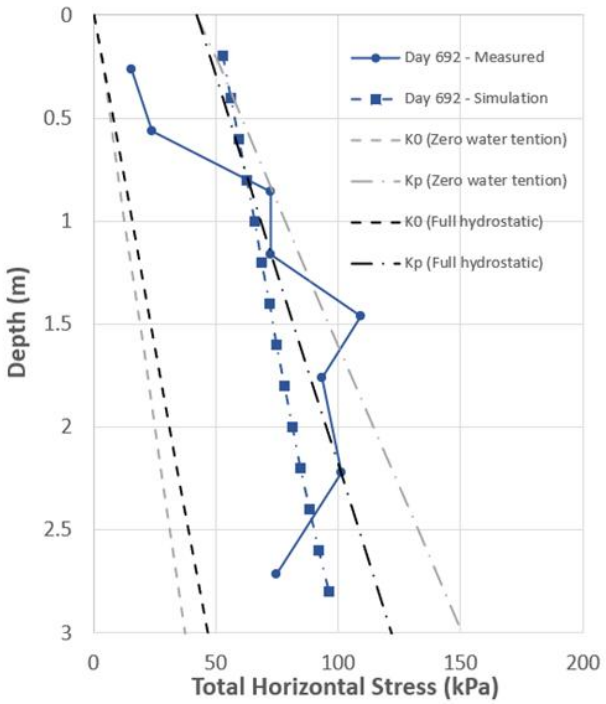

Figure 18. *Measured and simulation pressures on wall for Clayton et al. (1991) experiment.*

DOI: 10.4417/IJGCH-08-04-01

NUMERICAL SIMULATIONS OF TOP-DOWN WALLS RETAINING SWELLING SOILS

Top-down wall simulations were performed using two approaches: the finite difference method associated with the P-y curves analysis (RSPILE software) and the finite element method (CODE_BRIGHT software). In both cases, the simulated wall was the Brown (2013) cantilever wall case history described earlier.

Top-downRretaining Wall Simulation

Finite difference approach with RSPILE

The top-down cantilever wall of Brown (2013) was simulated using the finite difference technique with the RSPILE software (2024). A pressure diagram was applied above the excavation and P-y curves were input in the embedded portion of the wall. The goal was to match, as closely as possible, the final measured deflection (Figure 19). Seven different cases were simulated and are summarized in Table 3. The pressure diagram above the excavation level considered different possibilities, including the active earth pressure, the swell pressure, superposition of both, and a fraction of the swell pressure. The P-y curves below the excavation included two different approaches: pressuremeter P-y curves (Briaud, 2023b) and Reese P-y curves (Brown, 2013). The case which gave the best fit of the measured deflection profile (Figure 19) was Case 7 in Table 3. It was obtained by trial and error (7 cases in Table 3), while adhering to earth pressure principles and realistic judgement. Case 7 is described next in some detail.

The wall was simulated by using the reproducible wall section which is 0.762 m wide (drilled shaft diameter plus window between shafts) with the bending stiffness of a 0.61 m diameter drilled shaft. This bending stiffness was calculated to be 9.08 x 107 kN.m for the uncracked section, and 2.44 x 107 kN.m for the cracked section. The pressure above the ground water level (2.44 m depth) was chosen to be independent of the displacement (flat P-y curve). Since the measured swell pressure profile increased linearly with depth, the pressure within the top 2.44 m was chosen to be a linearly increasing profile of a fraction (21%) of the laboratory measured swell pressure. The 21% fraction was obtained by trial and error of a best match between the measured and predicted profile of deflection versus depth. The pressure profile below the ground water level (GWL) but above the excavation was the active earth pressure (effective pressure plus hydrostatic below GWL) using the intact soil properties (not fully softened) as shown in Table 3, Case 1.

The P-y curves below the excavation level were pressuremeter (PMT) P-y curves estimated from the undrained shear strength profile according to Briaud (2023) with one modification. The modification was to use a zero resistance P-y curve at the excavation level. This was necessary because the measured deflection profile indicated a fair amount of deflection at the excavation level; it was not possible to create such a deflection with a regular stiff clay PMT P-y curve, as it would lead to a smaller deflection. The PMT P-y curves (Briaud, 2023b) for a cylindrical pile are elastic and perfectly plastic with a plastic plateau value equal to p_L x B_{pile} and a slope equal to 2.3 x E_{pmt}. The PMT limit pressure p_L was estimated as 7su (Briaud, 2023a) and the PMT modulus E_{pmt} as $120s_u$ (Bahmani, Briaud, 2021). The P value of these PMT P-y curves were then multiplied by 0.5 to include the in-line group effect of the drilled shaft wall (Briaud, 2013b).

DOI: 10.4417/IJGCH-08-04-01

Table 3. *Finite difference cases to match Brown (2013) cantilever wall experiment.*

CASE No.	Pressure diagram above excavation level	P-y curves below excavation level	Concrete section modulus	Soil properties used	Calculated top deflection (mm)	Measured top deflection (mm)
1	Full swell pressure diagram increasing linearly with depth corresponding to the lab-measured swell pressures – no active pressure.	Pressuremeter elastic plastic P-y curves using $p_L = 7s_u$ and initial slope P/y = 276 s_u further reduced by 50% for in-line group	Uncracked section and then cracked section	Swell pressure p_{sw} = 57 kPa at z = 1.5 mm and p_{sw} = 182 kPa at z = 4.6 m. Undrained shear strength s_u = 76.6 kPa at excavation level and s_u = 287.3 kPa at bottom of wall	160.8 mm for uncracked section, more than 300 mm for cracked section. 41% of swell pressure matches the top deflection for the cracked section but not the complete deflection shape	132.8 mm at top of wall and 72.6 mm at excavation level.
2	Active triangular earth pressure plus hydrostatic water pressure with GWL at ground surface	Same as Case 1	Uncracked section and then cracked section	Fully softened shear strength friction angle = 24°, zero cohesion to be consistent with Brown 2013 final recommendations. Undrained shear strength same as case 1	48.0 mm for uncracked section and 110.7 mm for cracked section	132.8 mm at top of wall and 72.6 mm at excavation level
3	Same as Case 2 but GWL at 2.4 m depth	Same as Case 1	Uncracked section and then cracked section	Same as Case 2	32.1 mm for uncracked section and 71.7 mm for cracked section	132.8 mm at top of wall and 72.6 mm at excavation level
4	Same as Case 1 with full swell pressure but plus active earth pressure and hydrostatic pressure	Same as Case 1	Uncracked section and then cracked section	Same as Case 1 for swell pressure. Same as case 2 for active pressure. Same as case 1 for P-y curves	83.0 mm for uncracked section and 222.0 mm for cracked section	132.8 mm at top of wall and 72.6 mm at excavation level
5	Same as Case 2 but the P-y curves below excavation are those of Brown (2013)	Reese P-y curve for sand with φ= 30° and a group reduction factor equal to 0.62 as suggested by Brown (2013)	Elastic-plastic cracked section	Initial slope of P-y curve = 101.8 kN/m^3.	88.5 mm for the elastic plastic cracked section	132.8 mm at top of wall and 72.6 mm at excavation level
6	Reduced swell pressure diagram with 21% of lab measured swell pressure above the excavation	Reduced pressuremeter P-y curves. Same as Case 1 but with zero resistance at the excavation level and 50% of p_L at wall bottom	Elastic plastic cracked section	Same as Case 1	133 mm for the elastic plastic cracked section. The whole deflection profile matches well the measurements	132.8 mm at top of wall and 72.6 mm at excavation level
7	Reduced swell pressure diagram with 28% of lab measured swell pressure above GWL and active earth pressure plus hydrostatic water pressure below that	Same as case 6. Reduced pressuremeter P-y curves. Same as Case 1 but with zero resistance at the excavation level and 50% of p_L at wall bottom	Elastic-plastic cracked section	Same as Case 1	133 mm for the elastic plastic cracked section. The whole deflection profile matches very well the measurements	132.8 mm at top of wall and 72.6 mm at excavation level

DOI: 10.4417/IJGCH-08-04-01

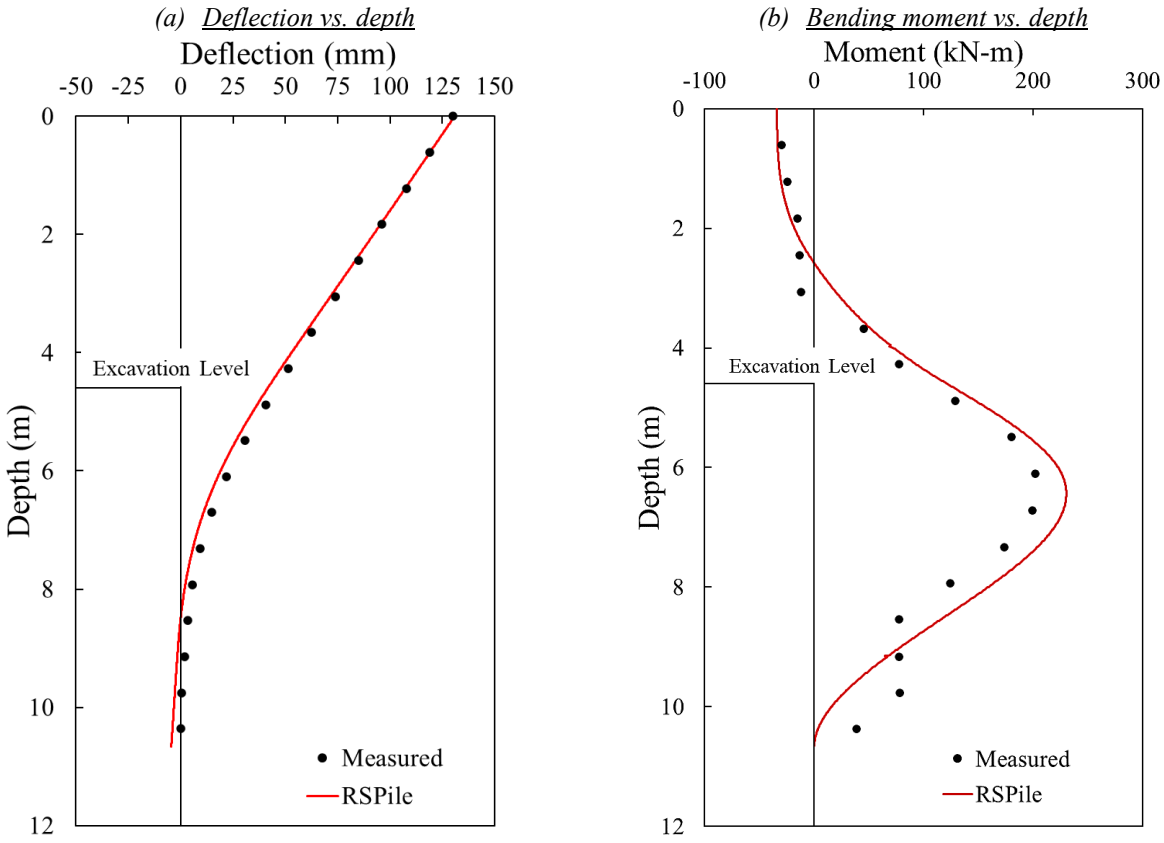

Figure 19. *Measured and fitted profiles for Brown (2013) wall corresponding to Case 6 in Table 3: (a) Deflection, (b) Bending moment (measured data from Brown, 2013).*

Finite element approach with Code Bright

The top-down cantilever wall tested by Brown (2013) was also simulated by using the software CODE_BRIGHT. The input parameters for the simulation were obtained by matching the field and lab tests results, such as particle size distribution, in-situ moisture content and total unit weight, permeability tests and direct shear tests. The model parameters were validated against swelling pressure laboratory tests. The mesh dimensions are shown in Figure 20. The loading and subsequent inundation sequences followed the full-scale wall testing sequence. To impose the wall's mechanical boundary conditions, we adapted the mixed von Neumann and Cauchy type boundary conditions available in CODE_BRIGHT (CODE_BRIGHT Manual, 2023). These conditions allow us to address situations that fall between the two typical extreme cases of "no movement" and "free to move," as in the example analyzed here.

The top deflection of the wall versus time shown in Figure 5b is repeated in Figure 21, along with the simulation results. Point O to Point A corresponds to the 4.6 m excavation. Point A to Point B corresponds to time-dependent movement only without any weather simulation. Point B to Point C to Point D corresponds to the first forced inundation (2 months). Point D to Point E corresponds to a no-action period with only time-dependent movement. Point E to Point F corresponds to the second forced inundation (4 months). The measured data shows, and the simulation confirms, that apart from the initial excavation, it is the inundation which created most of the deflection. As such, any guidelines should be based on the soil swelling process.

DOI: 10.4417/IJGCH-08-04-01

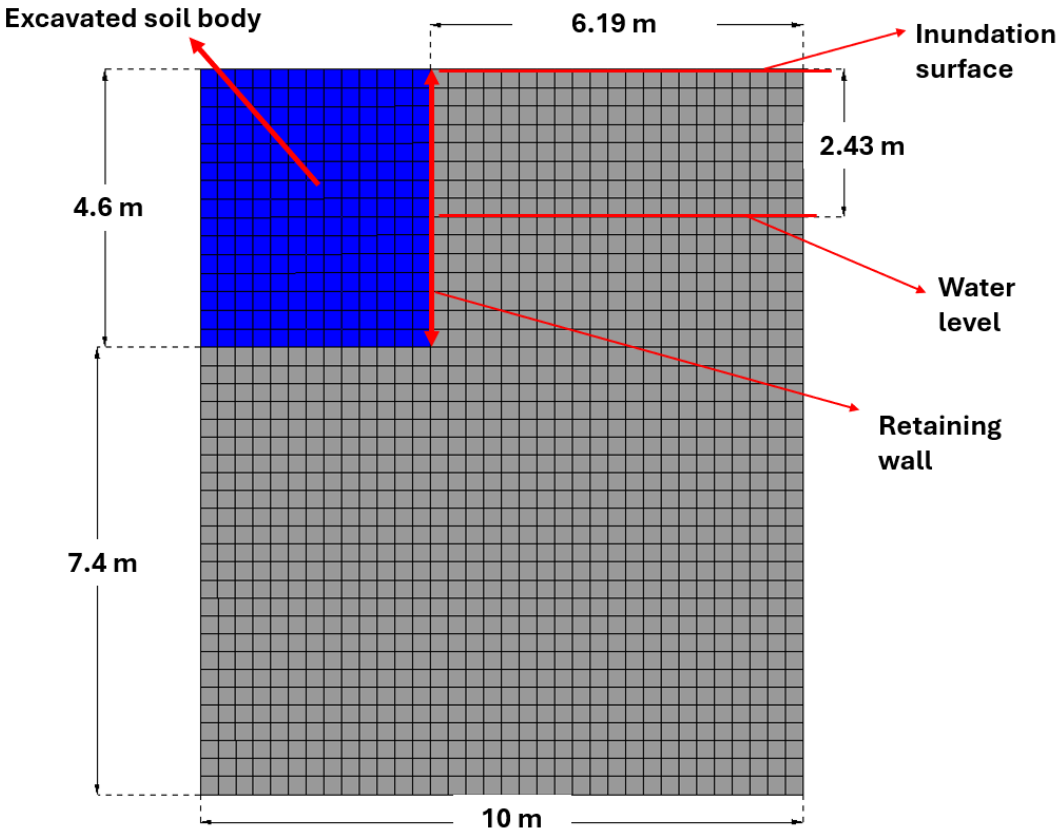

Figure 20. *Mesh dimensions.*

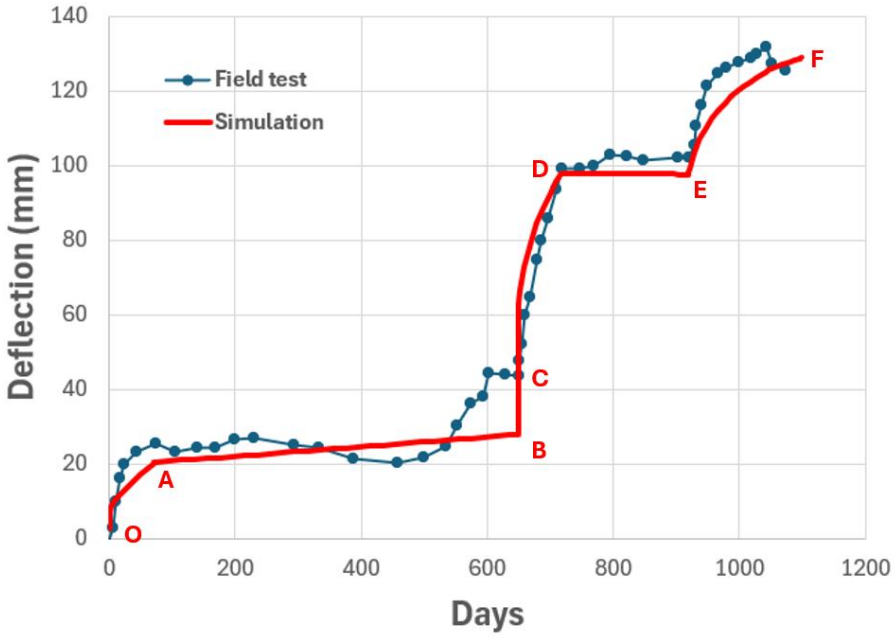

Figure 21. *Measured and predicted movement of the top of the wall (measurements from Brown, 2013).*

DOI: 10.4417/IJGCH-08-04-01

CHOICE OF A DESIGN EVENT FOR CALCULATING THE WALL PRESSURE

As was shown, the pressure developed against the wall by swelling depends on the time of inundation and on the permeability of the soil. The permeability of the soil can be obtained by testing. The question is to know what a reasonable period of inundation is for design purposes. To answer this question, the concept of the return period for a rainy period was developed as follows. The 100-year flood is a flood which has a probability of 0.01 or 1% in any one year of being exceeded. Similarly, the 100-year rainy period is defined here as the number of consecutive rainy days, which corresponds to a probability of exceedance of 0.01 in any one year. A rainy day is defined in a number of ways:

1. a day with a precipitation larger than zero
2. a day with a precipitation larger than 25 mm
3. a day with a precipitation larger than 50 mm
4. a day with a precipitation larger than 75 mm

A simple way to obtain this 100-year rainy period is described next by using an example. It follows the semi log plot approach for flood frequency analysis. Figure 22 presents the daily precipitation record in Houston from 1950 to 2023, or for a span of 73 years. For each year, the longest number of rainy days in a row is tabulated. Then, the longest annual rainy periods are organized and ranked in the descending order of number of days for the 73 years. The probability of exceedance is calculated for each year as the rank divided by the number of observations plus 1. A plot of the number of yearly rainy periods (number of rainy days) versus the decimal logarithm of the probability of exceedance is prepared (Figure 23). A regression line is fitted to the data, and the number of days corresponding to a chosen probability of exceedance can be obtained (Table 4). If one wishes to be consistent with many hydraulic designs, the 100-year return period can be chosen; for Houston, the 100-year rainy period would be 10 days with any rain, 4 days with at least 25 mm of rain, 3 days with at least 50 mm of rain, and 2 days with at least 75 mm of rain. The FEM simulations for the bottom-up wall and the top-down wall considered an inundation period, which means that water is ponded behind the wall for that many days. The question is how much rain per day would lead to a 24-hour inundation. It seems reasonable to assume that a significant amount of rain would be necessary; thus, the rainy period in Houston would be, at most, a few days.

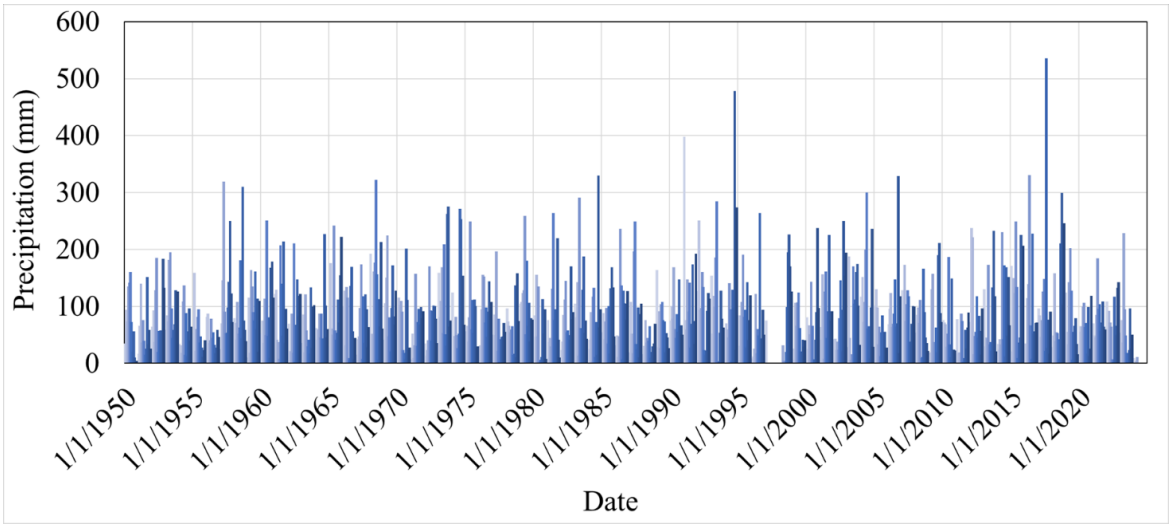

Figure 22. *Daily rainfall in Houston, Texas, from 1950 to 2023 (NOAA records).*

DOI: 10.4417/IJGCH-08-04-01

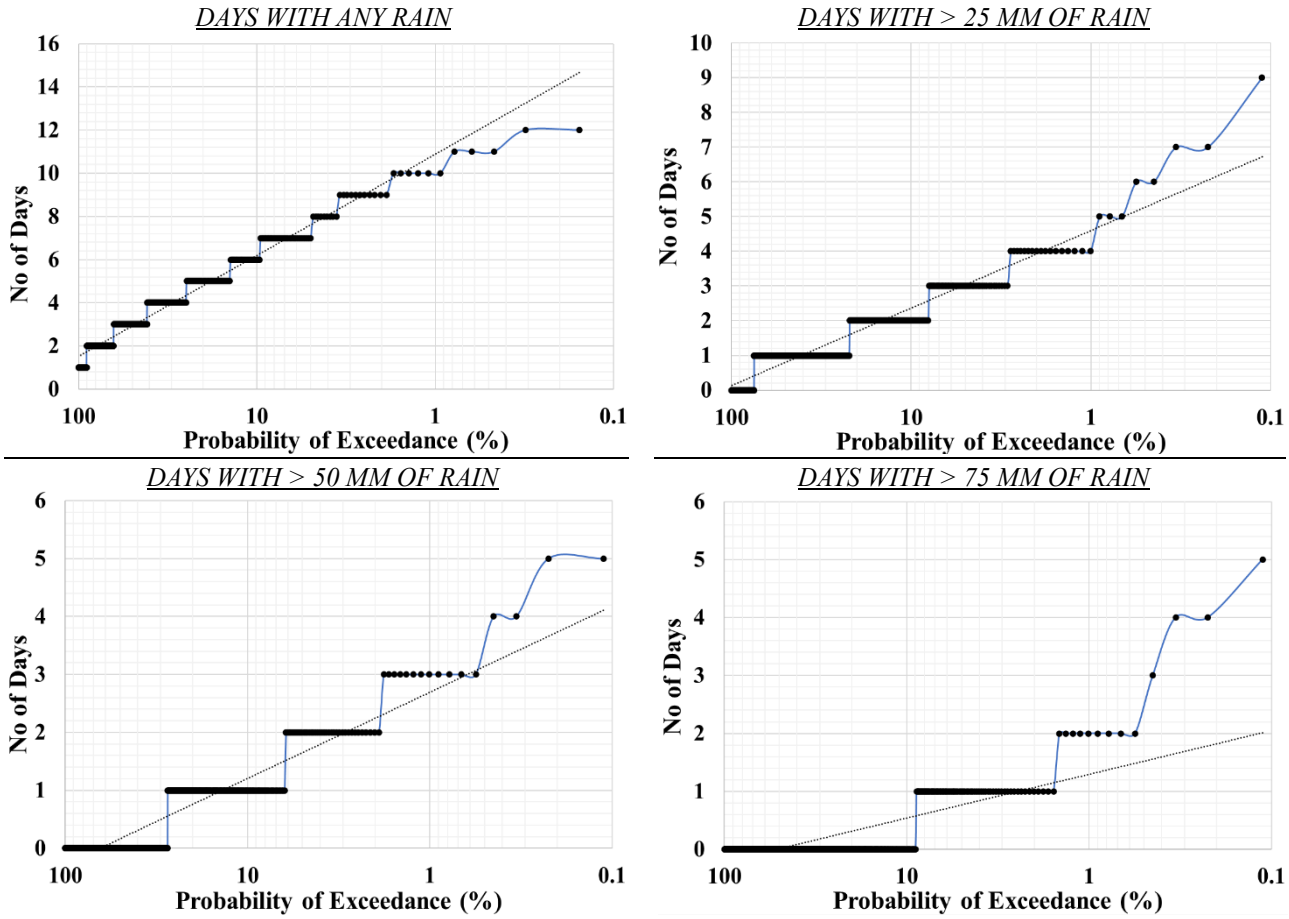

Figure 23. *Continuous rainy period in days versus probability of exceedance in percent for Houston, Texas (1950-2023).*

Table 4. *Number of rainy days for Houston, Texas, for the 100-year return period.*

Any rain	Days with > 25 mm of rain	Days with > 50 mm of rain	Days with > 75 mm of rain
10	4	3	2

DISCUSSION AND CONCLUSION

The pressure on walls retaining low water content swelling soils which become inundated can be much higher than the pressure on walls retaining non-swelling soils. The maximum possible pressure is the passive earth pressure of the soil. Above the ground water level, this passive earth pressure should be calculated by assuming zero water stress as the inundation decreases the suction to zero. The swell pressure is another limiting pressure. A review of four correlating equations to predict the swell pressure from common laboratory soil properties helps to identify the best correlation equation. The best predictions are given by the average predictions of the four selected equations.

The maximum pressure at any depth above the ground water level for a very long period of inundation is the smaller of the passive earth pressure and the swelling pressure. The minimum pressure at any depth is taken here as the at-rest earth pressure with zero water stress. The maximum pressure diagrams are illustrated in Figure 13. The time duration of the inundation period is critically important and the concept of a design inundation period corresponding to a chosen recurrence interval is

DOI: 10.4417/IJGCH-08-04-01

proposed. This concept is similar to the selection of a flood such as the 100-year flood for design purposes. The process to obtain the 100-year inundation period is outlined and is found to be between 2 and 10 days for Houston, Texas, depending on how much rain is considered to be sufficient to create complete around-the-clock inundation.

A non-dimensional time factor is proposed to regroup the influence of the soil permeability, the inundation time, and the wall height. Plots of pressure against the wall as a function of the time factor are suggested, and an example pressure diagram using that concept is presented. The wall movement is found to reduce the wall pressure by 30-50%. However, the wall pressure does increase with time and, for very long inundation periods, can go back to the no-movement condition.

Based on matching the measured and simulated displacement profile of a full-scale instrumented cantilever wall, it is shown that even after 6 months of inundation, only 21% of the swell pressure is applied by the soil to the wall. Therefore, for a reasonable number of rainy days and for a soil permeability consistent with high swelling potential soils, it is unlikely that the pressure behind a wall retaining low water content swelling soils will lead to a significantly higher pressure compared to non-swelling soils.

All in all, the major difference in pressure distribution between a wall retaining non-swelling soils and a wall retaining inundated swelling soils with low initial water content is that the pressure near the top of the wall can be larger in the latter case. If such a situation is not addressed, this could lead to the wall tipping over (Figure 22). In this case, the best solution is to place an anchor near the top of the wall to resist the added pressure if the soil swells. Another solution is to place a thick vertical compressible joint material immediately behind the wall to absorb, by compression, the pressure generated by the soil and thus not transfer the pressure to the wall.

Figure 22. *Wall retaining swelling soil with long-term inundation by a lawn watering system.*

DATA AVAILABILITY

Some or all data, models, or code that support the findings of this study are available from the corresponding author upon reasonable request.

ACKNOWLEDGMENTS

This project was sponsored by the Center for Education and Research in Geo-Engineering Practice (CERGEP). CERGEP members who contributed to this project are A.H. Beck, Corsair, Fugro, Geosyntec, Intertek-PSI, Kiewit, Menard, Odin, Paradigm, Raba-Kistner, Reinforced Earth, Riner Engineering, and Terracon.

DOI: 10.4417/IJGCH-08-04-01

REFERENCES

Abdollahi, M., and Vahedifard, F. (2021). Model for Lateral Swelling Pressure in Unsaturated Soils. *Journal of Geotechnical and Geoenvironmental Engineering*. https://doi.org/10.1061/(ASCE)GT.1943-5606.0002605

Alonso, E.E., Gens, A., & Josa, A. (1990). A constitutive model for partially saturated soils. *Géotechnique*, *40*(3), 405–430.

Bahmani, M., & Briaud, J.-L. (2021). Settlement of Foundations on Clay – A database study. In *Proceedings of the International Foundation Congress and Equipment Exposition (IFCEE)* (GSP 326). ASCE.

Bilgin, Ö., & Mansour, E. (2013). Anchored sheet pile wall design in expansive soils. In *Proceedings of the 18th International Conference on Soil Mechanics and Geotechnical Engineering* (pp. 1943–1946). Paris, France.

Briaud, J.-L. (2013). The Pressuremeter Test: Expanding its use. In *Proceedings of the 18th International Conference on Soil Mechanics and Geotechnical Engineering.* Paris, France.

Briaud, J.-L. (2023a). Geotechnical Engineering: Unsaturated and Saturated Soils (2nd ed). John Wiley and Sons.

Briaud, J.-L. (2023b). *Pressuremeter and foundation design* [Short-course notes]. Roctest.

Brown, A. C. (2013). *The behavior of drilled shafts retaining walls in expansive clay soils* [Doctoral dissertation, University of Texas at Austin].

Canadian Geotechnical Society. (2006). *Canadian foundation engineering manual* (4th ed.). Canadian Geotechnical Society.

Clayton, C. R. I., Symons, I.F., & Hiedra-Cobo, J.C. (1991). The Pressure of Clay Backfill Against Retaining Structures. *Canadian Geotechnical Journal, 28*(2), 282–297.

CODE_BRIGHT user's manual. (2023). Technical University of Catalonia.

Ellis, T. B. (2011). *A Subsurface Investigation in Taylor Clay* [Master's thesis, University of Texas at Austin].

Fourie, A. (1989). Laboratory evaluation of lateral swelling pressure. *Journal of Geotechnical Engineering, 115*(10), 1481–1489.

Gu, X. W. (2005). *Study on the interaction between unsaturated expansive soils and structure* [Master's thesis, Nanjing Hydraulic Research Institute]. (In Chinese)

Habib, S. A., & Karube, D. (1993). Swelling Pressure Behavior Under Controlled Suction. *Geotechnical Testing Journal, 16*(2), 271–275.

Hong, G. T., Aubeny, C. P., & Lytton, R. L. (2010). Lateral Earth Pressure on a Wall in expansive Soils. In *Proceedings of the International Conference on Unsaturated Soils.* CRC Press.

Joshi, R. P., & Katti, R. K. (1980). Lateral Pressure Development Under Surcharge. In *Proceedings of the 4th International Conference on Expansive Soils* (Vol. 1, pp. 227–241). ASCE.

Kate, J. M., & Katti, R. K. (1980). Effect of CNS Layer on the Behavior of Underlying Expansive Soil – an Experimental Study. *Indian Geotechnical Journal, 10*(4), 281–305.

Katti, R. K., Bhangale, E. S., & Moza, K. K. (1983). *Lateral Pressure in Expansive Soil with and without a Cohesive Non-Swelling Soil Layer - Application to Earth Pressures on Cross Drainage Structures in Canals and Key Walls in Dams (Studies on Ko Condition).* (Technical Report No. 32). Central Board of Irrigation and Power.

Komornik, A., & David, D. (1969). Prediction of Swelling Pressure of Clays. *Journal of the Soil Mechanics and Foundations Division, 95*, 209–226.

Kormornik, A., & Zeitlen, J. G. (1965). An Apparatus for Measuring Lateral Soil Swelling Pressure in the Laboratory. In *Proceedings of the 6th International Conference on Soil Mechanics and Foundation Engineering* (Vol. 1, pp. 278–281).

Liu, Y., & Vanapalli, S. K. (2017). Influence of Lateral Swelling Pressure on the Geotechnical Infrastructure in Expansive Soils. *Journal of Geotechnical and Geoenvironmental Engineering.* https://doi.org/10.1061/(ASCE)GT.1943-5606.0001651

DOI: 10.4417/IJGCH-08-04-01

Liu, Y., & Vanapalli, S.K. (2019). Prediction of Lateral Swelling Pressure Behind Retaining Structures with Expansive Soil as Backfill. *Soils and Foundations, 59*(1), 176–195. https://doi.org/10.1016/j.sandf.2018.10.003

Liu, Z., Zhang, R., Liu, Z., & Zhang, Y. (2021). Experimental Study on Swelling Behavior and Its Anisotropic Evaluation of Unsaturated Expansive Soil. *Advances in Materials Science and Engineering, 2021*, 13. https://doi.org/10.1155/2021/6937240

McCormack, D. E., & Wilding, L. P. (1975). Soil Properties Influencing Swelling in Canfield and Geeburg Soils. *Soil Science Society of America Journal, 39*(3), 387–598.

Mohamed, O. Z., Taha, Y. K., & Abd El-Aziz, E. M. (2014). Field Study of The Distribution of Lateral Swelling Pressure of Expansive Soil on Retaining Structure. *Journal of Engineering Sciences, 42*(2), 289–302.

Moore, P. J., & Spencer, G. K. (1972). Lateral Pressures from Soft Clays. *Journal of the Soil Mechanics and Foundations Division, 98*(11), 1225–1244.

NAVFAC DM 7.02. (1986). *Foundations and Earth Structures* (Design Manual No. 7.02). Naval Facilities Engineering Command, 279 pp.

Nayak, N., & Christensen, R. W. (1971). Swelling Characteristics of Compacted, Expansive Soils. *Clays and Clay Minerals, 19*, 251–261.

Ofer, Z. (1981). Laboratory Instrument for Measuring Lateral Soil Pressure and Swelling Pressure. *Geotechnical Testing Journal, 4*(4), 177–182.

Olivella, S., Gens, A., Carrera, J., & Alonso, E. E. (1996). Numerical formulation for a simulator (CODE_BRIGHT) for the coupled analysis of saline media. *Engineering Computations, 13*(7), 87–112.

RSPILE. (2024). *Rocscience software for axial and lateral pile analysis.* Rocscience. https://www.rocscience.com.

Sánchez, M., Gens, A., & Guimarães, L. (2012a). Thermal-hydraulic-mechanical (THM) behavior of a large-scale in situ heating experiment during cooling and dismantling. *Canadian Geotechnical Journal, 49*(10), 1169–1195.

Sánchez, M., Gens, A, & Olivella, S. (2012b). THM Analysis of a large-scale heating test incorporating material fabric changes. *International Journal for Numerical and Analytical Methods in Geomechanics.* https://doi.org/10.1002/nag.1011

Schneider, G. L., & Poor, A. R. (1974). *The prediction of soil heave and swell pressures developed by expansive clay* (Research Report TR-9-74). Construction Research Centre.

Thomas, M.G., Puppala, A.J., and Hoyos, L.R. (2009). "Influence of swell pressure from expansive fill on retaining wall stability." *Proc., Intern. Found. Congr. & Equipment Expo 2009*, Orlando, Fla., GSP 187, 590-597.

van Genuchten, R. (1978). Calculating the unsaturated hydraulic permeability conductivity with a new closed-form analytical model. *Water Resources Research, 37*(11), 21–28.

Zhang, R., Liu, Z., Zheng, J., & Zhang, J. (2019). Experimental Evaluation of Lateral Swelling Pressure of Expansive Soil Fill behind a Retaining *Journal of Materials in Civil Engineering, 32*(2), 04019360.

APPENDIX

Example Calculations

The following example helps explain how to use the proposed guidelines. The wall height is 5 m, the soil is a swelling soil with a permeability of $5x10^{-10}$ m/s and a swell pressure is 150 kPa, and the inundation time is 2 days. The time factor β is:

$$\beta = \frac{5\times10^{-10}\times3\times24\times3600}{5} = 2.6\times10^{-5} \quad (17)$$

The position of the pressure diagram for β = 2.6x10-5 is estimated from Figure 14(b) and represents the pressure diagram. The increase in pressure is located close to the ground surface and is quite small. If the increase in pressure was significant,

DOI: 10.4417/IJGCH-08-04-01

a shallow anchor would help minimize the wall from moving in a tip-over displacement. This anchor capacity could be calculated to resist the shallow pressure in excess of the at-rest earth pressure.

Mechanical Constitutive Model

The Barcelona Basic Model (BBM) was adopted to represent the mechanical behavior of the soil (Alonso et al., 1990). The model is formulated in terms of the three stress invariants (p; J; θ) and suction, defined as,

$$p = \left(\frac{1}{3}\right)\left(\sigma_x + \sigma_y + \sigma_z\right) \tag{A1}$$

$$J^2 = \tfrac{1}{2}\,\mathrm{trace}\left(\boldsymbol{s}^2\right) \tag{A2}$$

$$\theta = -\frac{1}{3}sin^{-1}\left(1.5\sqrt{3}\ det\ \boldsymbol{s}/J^3\right) \tag{A3}$$

with:

$$\boldsymbol{s} = \boldsymbol{\sigma} - p\boldsymbol{I} \tag{A4}$$

where I is the identity tensor.

The trace of the yield function on the isotropic p-s plane is called the *LC* (Loading-Collapse) yield curve because it represents the locus of activation of irreversible deformations due to loading increments or wetting (collapse compression). The position of the *LC* curve is given by the value of the hardening variable p_o*. The *BBM* yield surface (*F*) is then expressed as:

$$F = 3J^2 - \left[\frac{g(\theta)}{g(-30^{\circ})}\right]^2 M^2(p + p_s)(p_0 - p) = 0 \tag{A5}$$

When yielding takes place, the increment of plastic deformations is evaluated through:

$$\dot{\boldsymbol{\varepsilon}}^p = \lambda\frac{\partial G}{\partial \boldsymbol{\sigma}} \tag{A6}$$

where G is the plastic potential as follows:

$$G = \alpha_G 3J^2 - \left[\frac{g(\theta)}{g(-30^{\circ})}\right]^2 M^2(p + p_s)(p_0 - p) = 0 \tag{A7}$$

where α_G is the material parameter that controls the degree of non-association, determined according to (Alonso et al., 1990).

The hardening law is expressed as a rate relation between the volumetric plastic strain and the saturated isotropic pre-consolidation stress 'p^*_0', according to:

DOI: 10.4417/IJGCH-08-04-01

$$\frac{\dot{p}_0^*}{p_0^*} = \frac{(1+e)}{(\lambda_{(0)} - \kappa)} \dot{\varepsilon}_v^p \tag{A8}$$

The dependence of the tensile strength on suction is given by:

$$p_s = ks \tag{A9}$$

The dependence of p_0 on suction is given by:

$$p_0 = p_c \left(\frac{p_0^*}{p_c}\right)^{\frac{\lambda_{(0)}-\kappa}{\lambda_{(s)}-\kappa}} \tag{A10}$$

The compressibility parameter for changes in net mean stress for virgin states of the soil ($\lambda_{(s)}$) depends on suction according to:

$$\lambda_{(s)} = \lambda_{(0)}[r + (1-r)\,exp(-\beta s\ )] \tag{A11}$$

The bulk modulus (K) for changes in mean stress is evaluated with the following law:

$$K = \frac{(1+e)}{\kappa} p \tag{A12}$$

The bulk modulus for changes in suction is computed according to the following law:

$$K_s = \frac{(1+e\ )(s\ + p_{atm})}{\kappa_s} \tag{A13}$$

The variation of stress-stiffness with suction and the variation of swelling potential with stress and suction have been considered. The resulting elastic volumetric strain is obtained through:

$$\dot{\varepsilon}_v^e = \frac{\kappa}{(1+e)}\frac{\dot{p}}{p} + \frac{\kappa_S}{(1+e)}\frac{\dot{s}}{(s+0.1)} \tag{A14}$$

and the elastic deviatoric strain is obtained as:

$$\dot{\varepsilon}_s^e = \frac{\dot{J}}{G_t} \tag{A15}$$

DOI: 10.4417/IJGCH-08-04-01

where (CODE_BRIGHT Manual, 2023):

$$\kappa = \kappa_i(1 + \alpha_s s) \tag{A16}$$

$$\kappa_s = \kappa_{s0}\left(1 + \alpha_{sp}\, ln\, p\, /p_{ref}\right) \tag{A17}$$

$$G_t = \frac{3(1-2\mu)K}{2(1+\mu)} \tag{A18}$$

Constitutive Models Related to the Hydraulic Behavior

Advective fluxes are computed using the generalized Darcy's law, expressed as:

$$\boldsymbol{q}_l = -\boldsymbol{K}_l(\nabla P_l - \rho_l \boldsymbol{g}); \tag{A19}$$

The permeability tensor is evaluated according to:

$$\boldsymbol{K}_l = \boldsymbol{k}\frac{k_{rl}}{\mu_l} \tag{A20}$$

The dependence of intrinsic permeability on porosity has been based on Kozeny's law (Sanchez et al.., 2012b):

$$\boldsymbol{k} = k_0 \exp[\mathrm{b}(n_0 - n_0)]\boldsymbol{I} \tag{A21}$$

The well-known power law has been adopted to describe the dependence of liquid permeability on degree of saturation:

$$k_{rl} = {S_l}^{n_s} \tag{A22}$$

A value of ns = 3 was adopted. The water retention curve relates the degree of saturation of the material with suction. The law adopted is based on the van Genuchten model (van Genuchten, 1978), as follows:

$$S_l = \left[1 + \left(\frac{s}{P_o}\right)^{\frac{1}{1-\lambda_o}}\right]^{-\lambda_o} \tag{A23}$$

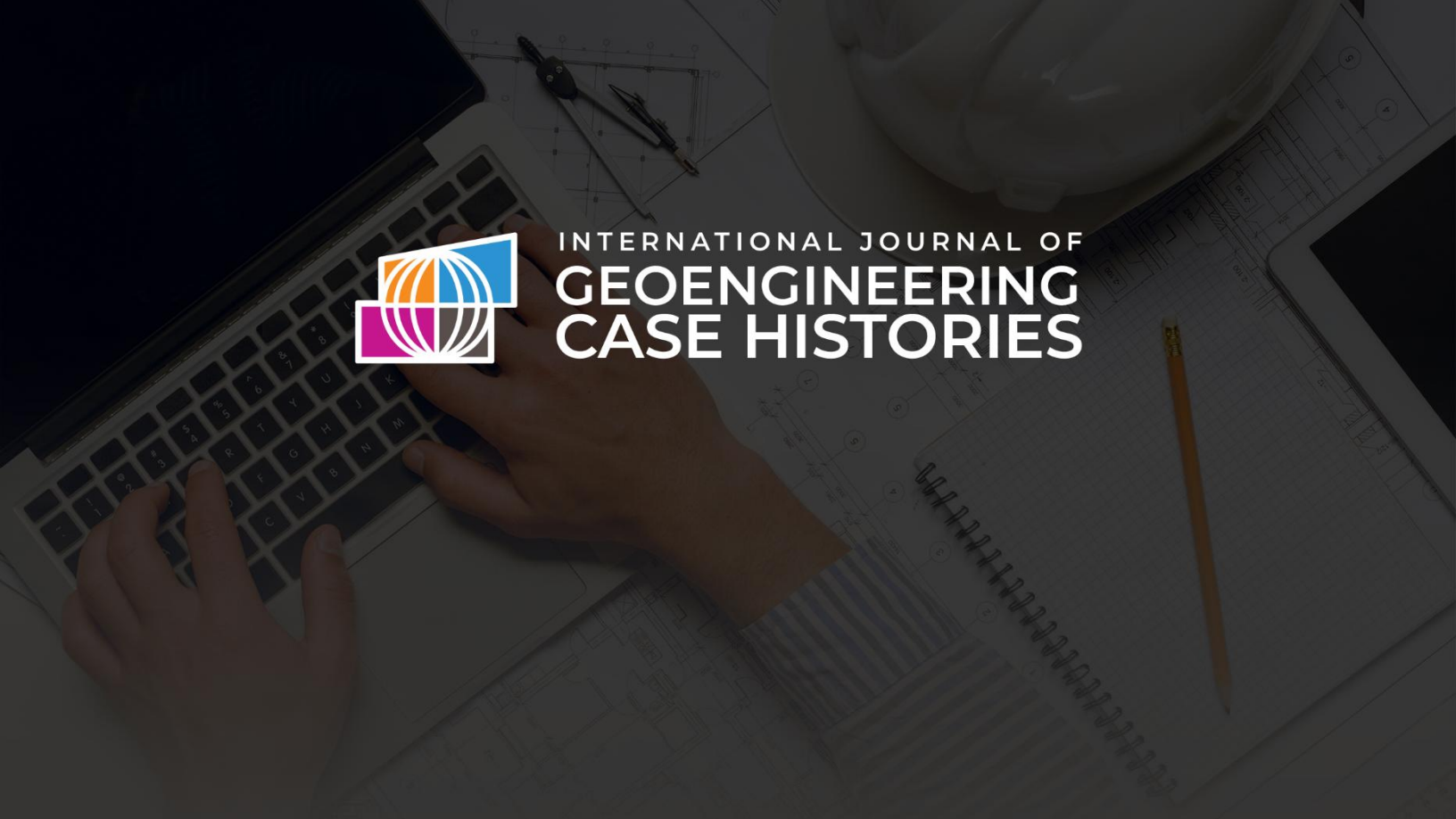

INTERNATIONAL JOURNAL OF
GEOENGINEERING
CASE HISTORIES

The Journal's Open Access Mission is generously supported by the following Organizations: